International Journal of Fracture **70:** 275–304, 1995.

Near-tip dual-length scale mechanics of mode I cracking in laminate brittle matrix composites

R. BALLARINI[1], P. G. CHARALAMBIDES[2] and S. ISLAM[1]
[1] *Department of Civil Engineering, Case Western Reserve University, Cleveland, Ohio 44106-7201, USA*
[2] *Department of Mechanical Engineering, The University of Maryland, Baltimore County, Baltimore, MD 21228, USA*

Received 15 August 1994; accepted 24 January 1995

Abstract. This paper presents the results of a numerical study on the near-tip mechanics of mode I cracking in brittle matrix composite laminates. A finite element model is developed within the context of two competing characteristic lengths present in the composite, i.e., the microstructural length such as the layer thickness and the macro-length such as the crack length, uncracked ligament size, etc.. The crack surfaces are assumed to be traction free and perpendicular to the reinforcing layers. Conditions leading to macroscopic homogeneous orthotropic mechanical behavior are also assumed. Thus, the near-tip numerical studies are carried out within a small-scale heterogeneous zone which surrounds the crack tip and is dominated at its outer boundary by the displacements associated with a mode I crack in a homogeneous orthotropic medium. The model is used to calculate the stresses and stress intensities in the vicinity of the crack tip which develop due to the alternating fiber/matrix heterogeneous composite microstructure. Parameter studies elucidating the effects of the two competing composite characteristic lengths on the evolution and structure of the near-tip heterogeneous stress fields are carried out. The results indicate that when the characteristic microstructural length is relatively large compared to the macroscopic length, the singular heterogeneous stress fields may deviate substantially from the assumed homogenized orthotropic fields. The study can be used to determine the necessary conditions under which homogenization applies in obtaining an accurate description of the stresses in the vicinity of the crack tip in a laminated composite.

1. Introduction

A significant amount of research has been conducted aimed at gaining better understanding of the fracture mechanics of Brittle Matrix Composites (BMCs). Some of the earlier work [1–3] concentrated on the development of models which could be used to predict the first matrix cracking stress under mode I loading conditions. These models addressed primarily fiber reinforced systems and were developed utilizing the mechanics of a fundamental fiber/matrix unit cell subjected to remote tension. More recently the problems of stability of fiber failure [4–6], fiber debonding [7–8] and delamination in composite laminates [9, 10] have been addressed.

For mode I problems in which the crack propagates in a direction which is perpendicular to the fiber reinforcement, various techniques have been used to solve for the stress intensity factor driving the matrix crack. For example, in accordance with the 'unit cell' models the onset of crack growth is assessed with the aid of a K^{ortho}-dominated local zone, the extent of which is controlled by the composite microstructure, such as the fiber or the composite cylinder diameter for fiber reinforced composites, or the layer thickness in composite laminates shown in Fig. 1a. In other methods, the microstructure of the composite is smeared out and the material is modeled as homogeneous anisotropic consistent with Fig. 1b. To predict matrix cracking it is assumed that the local matrix stress intensity factor $K_{\text{I}}^{\text{tip}}$ (the stress intensity factor which exists when the crack tip is in the matrix) is related to the orthotropic K^{ortho}

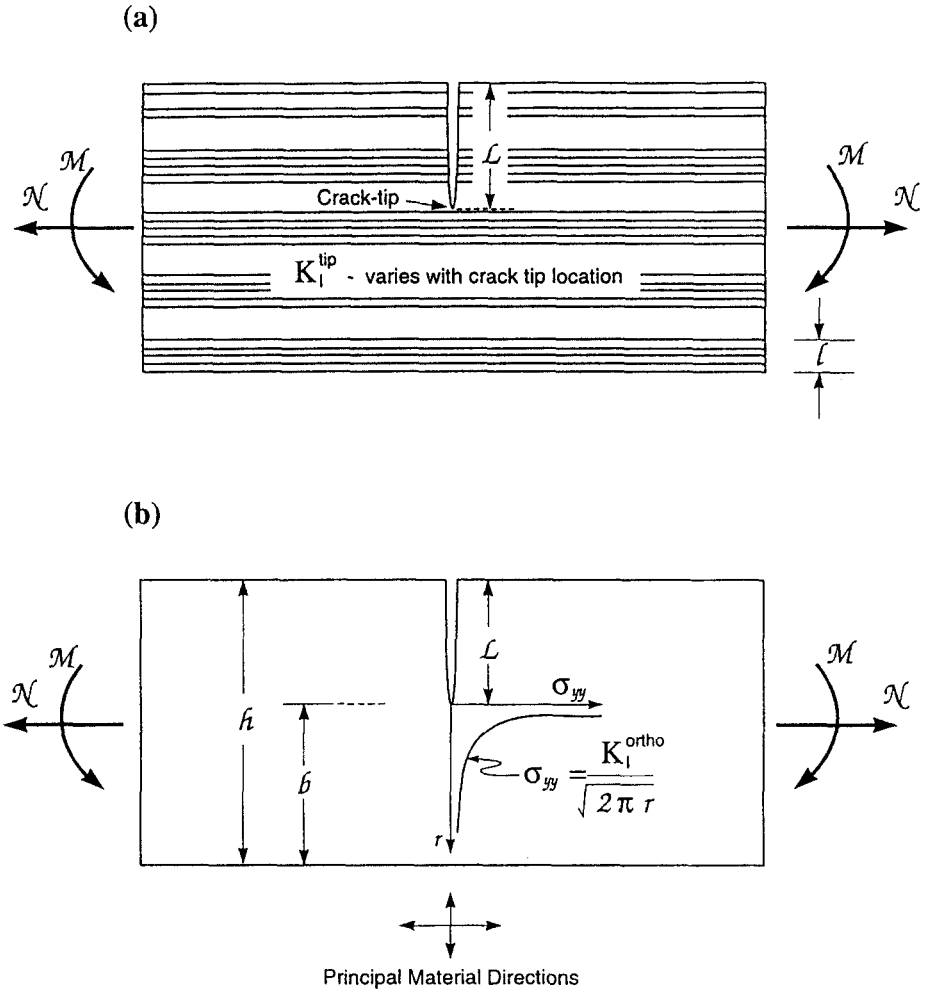

Fig. 1. (a) A cracked laminated beam. (b) A homogenized orthotropic cracked laminated beam.

through the relation $K_I^{tip} = K^{ortho} E_m / E_c$, where E_m and E_c represent the elastic moduli of the matrix and the composite respectively. This relation, which follows from the assumption that the rule of mixtures applies for stress intensity factors, implies that the stress and strain fields in the vicinity of the crack tip are dominated by K^{ortho} regardless of the details of the microstructure. Such an approach may be warranted for composite systems wherein the microstructural characteristic length is sufficiently smaller than its dual macroscopic characteristic length obtained from the finite specimen geometry. As discussed elsewhere [11], although such conditions may apply to fiber reinforced systems, it is very likely that they may be violated in composite laminate systems in which case a more thorough study of the near tip mechanics is warranted.

The present study addresses the near-tip mechanics of mode I cracking in brittle matrix composite laminates within the context of two competing characteristic lengths: the microstructural length ℓ and the macro-length L. The term 'dual length scale mechanics' arises from the competition between these lengths to characterize the near-tip singular stress field in the composite. As such, in this paper emphasis is placed on the mechanics governing the elastic singular stress

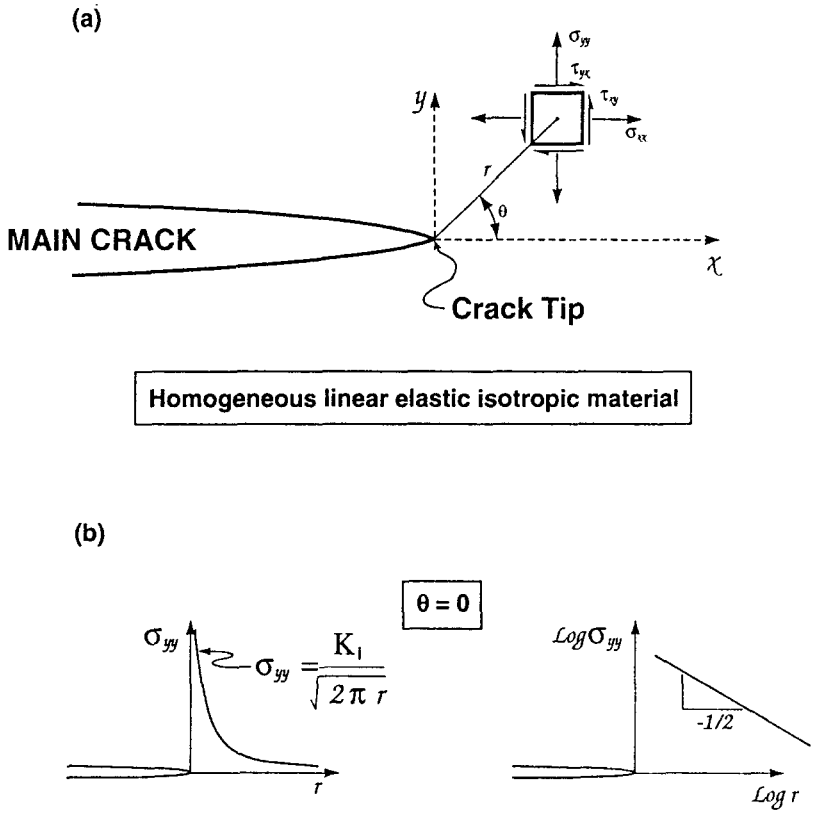

Fig. 2. (a) A schematic of a plane stress element embedded in the near-tip singular domain. (b) Normal stress profiles ahead of the crack tip as predicted via the near-tip asymptotics. The Log-Log scale reveals the square root singular character of the near-tip stresses.

fields in the vicinity of the crack tip embedded in a composite laminate. Consider the planar geometry of the cracked laminated beam shown in Fig. 1a. This geometry is representative of a typical fiber reinforced [0/90] cross ply laminate or any multilayer system with alternating homogeneous layers. In the case of fiber reinforced laminates, the 0° plies, also referred to as *fiber layers* or *fiber phase*, consist of layers with relatively stiff fiber reinforcements aligned along the length of the beam, whereas the 90° plies, also referred to as the relatively low stiffness *matrix phase*, may consist of layers reinforced with fibers aligned perpendicular to the plane shown in Fig. 1a. In this study, the crack is placed perpendicular to the 0° layers with its tip located in the matrix phase between two 0° layers. In addition, the laminated beam may be subjected to remote tension and bending. Under these loading conditions, a local stress intensity factor K_I^{tip} can be used to characterize the stress and displacement fields in the immediate vicinity of the crack tip. The zone dominated by K_I^{tip} is confined well within the matrix phase, extending to a distance from the physical crack tip equal to a fraction of either the layer spacing or the layer thickness ℓ. In any case, fracture of the matrix phase in the composite laminate is driven by this local stress field and thus K_I^{tip} should be the characterizing fracture parameter for matrix cracking. The traditional approach, however, used to characterize such fracture processes in brittle matrix fiber reinforced composites and composite laminates involves modeling the structure as a homogeneous orthotropic material as shown in Fig. 1b. This approach involves the use of a well defined orthotropic stress intensity factor K_I^{ortho} to

characterize the homogeneous orthotropic stress and displacement fields in the near-tip region. For $K_{\mathrm{I}}^{\mathrm{ortho}}$ to be relevant, the extent of its region of dominance should be much larger than the microstructural characteristic length ℓ; it should, however, be limited to a distance from the physical crack tip which is a fraction of the only available characteristic length in the modeled system, in this case the macro-length L or the uncracked ligament $b = h - L$. The following question arises: for which L/ℓ does this procedure lead to an accurate or acceptable description of the near-tip fields associated with the original structure? The present work is devoted to finding the answer to this question. More specifically, a near-tip finite element scheme is employed to calculate the heterogeneous stress field(s) in the vicinity of the crack tip and their associated stress intensity factor(s) while preserving the microstructural laminate morphology. Parameter studies involving the characteristic length ratio L/ℓ, the fiber volume fraction and constituent properties are carried out. The results are compared to those predicted using homogenization.

2. Near-tip mechanics and small scale perturbations

The most well known K-dominated near-tip stress fields are associated with cracks in homogeneous systems, and are obtained by solving the asymptotic, near-tip boundary value problem assuming a linear elastic response and ideally sharp crack tip geometric conditions [12]. The asymptotic linear elastic stress and strain fields exhibit an $r^{-1/2}$ singularity, with r being the radial distance from the crack tip shown in Fig. 2. These singular fields can be described through a single parameter K and universal spatial functions for each fracture mode, i.e., mode I or opening mode, mode II or in-plane shearing mode and mode III or anti-plane tearing mode. The stress intensity factors K_{I}, K_{II}, K_{III}, associate the intensity of the related stress and strain fields for each of the above modes of fracture to the applied loads and specimen geometry. The region of dominance of the above fields is limited by their singular character and extends to a distance r_0 from the physical crack tip equal to a fraction of some macroscopic specimen characteristic length L, such as the crack length, length of the uncracked ligament, or other characteristic specimen dimensions. Outside the K-dominated zone, other nonsingular solutions overwrite the diminishing near-tip fields rendering the latter fields meaningless.

As a means of adjusting to the singular stresses, a material responds locally in a nonlinear manner that effectively negates or perturbs substantially the elastic singularity in the immediate vicinity of the crack tip. The nonlinearities are unique to the material and may be associated with a number of different phenomena such as plastic yielding in metals [13] and microcracking damage [14] and phase transformation [15] in ceramics. Other mechanisms leading to ductile rupture in metal matrices [16–18] or failure of fiber/particle reinforced metal or brittle matrix composites [19, 20], may potentially be activated in the zone near the crack tip in various material systems. Clearly, upon application of the applied loads and at relatively small load levels, the material nonlinear response is limited to a small region surrounding the crack tip. As the applied loads increase, the nonlinear *process zone*, as signified by the active presence of any of the above mentioned or other nonlinear processes, spreads outwards from the crack tip, resulting in new, often nonsingular stress fields that develop inside the nonlinear process zone. From the near-tip mechanics viewpoint, the presence of the process zone helps establish an effective microstructural characteristic length, i.e., the process zone size r_p, which determines the extent of dominance of the new asymptotic stress fields within the process zone itself. It is worth emphasizing that the structure of the fields within the process zone may be significantly different from the K-fields. Small scale process zone conditions can be assumed when r_p

is considerably smaller than the singular elastic region dominated by K, i.e. $r_p \leqslant r_0/20$. Under these conditions, the influence of the process zone on the near-tip fields is limited to a small region in the immediate vicinity of the crack tip. This allows for a substantial annular region bounded by an inner radius which is a small multiple of r_p and an outer radius equal to r_0 where the singular elastic fields are still valid and remain virtually unaffected by the presence of the process zone. Under these conditions, K represents a valid stress and energy release rate characterizing parameter and can be used to assess fracture even in the presence of nonlinear processes within a small zone close to the crack tip. Similar ideas can be formulated for laminated heterogeneous systems as follows.

2.1. NEAR-TIP DUAL-LENGTH ASYMPTOTICS IN COMPOSITE LAMINATES

Consider the local-global representation of a cracked composite laminate shown in Fig. 3.

Let L represent the macroscopic length scale (crack length, uncracked ligament length, or any other relevant characteristic length), and let ℓ represent the microstructural length scale. In this study ℓ is taken as the thickness of the stiffer fiber reinforcing layer consistent with Figs. 1a and 3b. The crack surfaces are assumed to be traction-free, and the crack plane is taken to be perpendicular to the direction of the reinforcements. It is expected that for large values of L/ℓ, a near-tip, *small scale heterogeneous zone* exists and arguments analogous to those presented for small scale process zones can be used to study the evolution of the near-tip stress fields. For example, in small scale yielding, the near-tip plastic zones that develop with increasing loads disturb the singular elastic solution giving rise to other near-tip asymptotics such as the HRR fields in deformation plasticity and power law hardening materials [21, 22]. Similarly, it is expected that for the laminated composite problem the heterogeneity perturbs the singular fields predicted by the homogenized asymptotic solution giving rise to dual asymptotics consistent with the dual length scales present in the near-tip region.

Moreover, for large L/ℓ values, the mechanical response of the layered material at distances sufficiently away from the physical crack tip can be studied by *ignoring* the microstructure while employing the properties of a homogeneous orthotropic medium instead. The latter properties are usually extracted from the individual properties of the fiber and matrix constituents via a homogenization procedure. This approach often leads to the use of the rule of mixtures in extracting longitudinal properties and the inverse or a modified inverse rule of mixtures in extracting the transverse properties. In any case, the stresses associated with the response of the homogenized medium reflect average stress measures acting over the length of a microstructural unit fiber/matrix cell. The actual microstresses, can then be obtained by considering the deformation characteristics of the unit cell subjected to the overall orthotropic average stresses obtained for the homogenized system.

Under such conditions, the average unit cell stresses in the neighborhood of the crack tip are $r^{-1/2}$ singular and can be characterized via an orthotropic stress intensity factor $K_{\mathrm{I}}^{\mathrm{ortho}}$. The outermost radius r_3 from the physical crack tip of the zone dominated by $K_{\mathrm{I}}^{\mathrm{ortho}}$ is expected to depend on the macroscopic characteristic length L such that at least $r_3 \leqslant \frac{L}{20}$. Thus, in a homogenized medium, region III as shown in Fig. 3 is defined as being dominated by the homogeneous orthotropic singular stress field with $K_{\mathrm{I}}^{\mathrm{ortho}}$ being the characterizing parameter. While this may be a realistic approximation for material systems with large L/ℓ ratios one should also underscore that this approach may only provide useful stress field approximations at material points located within region III at distances from the physical crack tip which are much larger than the microstructural characteristic length ℓ. As a result of the heterogeneous

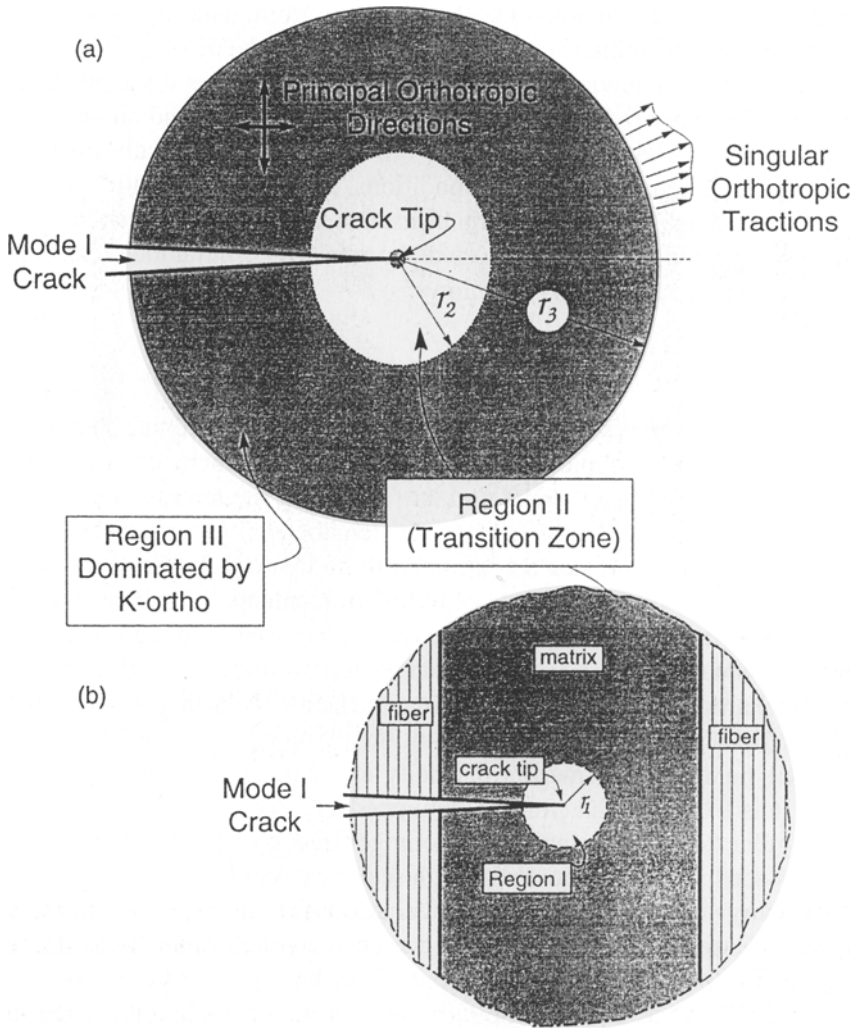

Fig. 3. (a) A schematic representation of small scale singular stress zone near the tip region of a mode I crack embedded in a fiber reinforced laminated brittle matrix composite. The material in Region III is treated as a homogeneous orthotropic continuum with its principal directions shown in Fig. 3a. (b) An enlarged cut-out domain from Fig. 3a depicting Region I which is dominated by the tip stress intensity factor $K_{\mathrm{I}}^{\mathrm{tip}}$.

microstructure, it is clear that distinctly different asymptotics will dominate the mechanics at material points in region I which contains the physical crack tip.

As shown in Fig. 3, the extent r_1 of region I from the crack tip depends on the position of the crack tip relative to the adjacent fiber layers and the degree of elastic mismatch, and it is a fraction of either the thickness of the fiber phase or the fiber phase spacing i.e. $r_1 \leqslant \ell/20$. For the sake of simplicity and without loss of generality, in the present study the crack tip is assumed to be within the matrix phase at the mid-point between two adjacent fiber layers. Thus, within region I, the singular stress field characterized by a local stress intensity factor $K_{\mathrm{I}}^{\mathrm{tip}}$, develops as if the fiber reinforcing phases were not present.

The distinct asymptotics dominating regions I and III discussed above are assumed to develop in heterogeneous systems with large L/ℓ ratios. In layered systems wherein the matrix and fiber are comprised of similar materials, the dominance of region I would clearly prevail

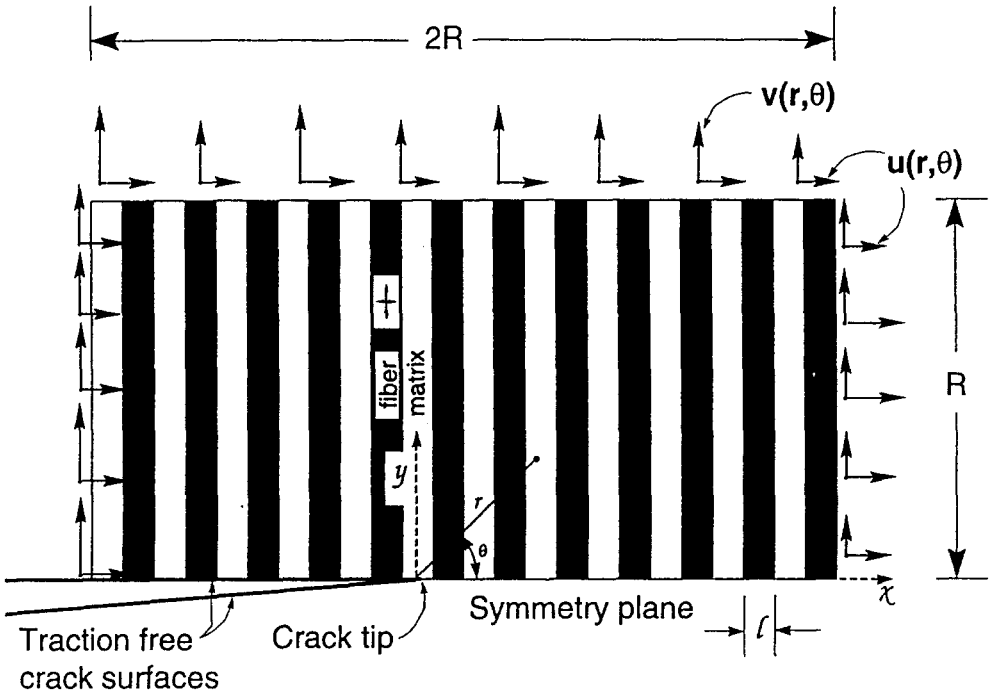

Fig. 4. Plane stress model used in the near-tip finite element studies. The arrows represent the homogenized orthotropic displacement components which are imposed as boundary conditions in the plane stress near-tip boundary value problem. The expressions for **u** and **v** are given in the Appendix.

over region III with r_1 extending to r_3. For heterogeneous systems, however, the asymptotic fields in regions I and III are expected to be matched through other fields dominating the transition region II which is also shown in Fig. 3.

The near-tip dual-length asymptotics discussed above are analogous to the small scale process zone concepts discussed earlier. Like plasticity for example, the fiber heterogeneities perturb the homogenized singular fields giving rise to local near-tip fields which may be distinctly different from those dominating region III. The region affected by the presence of the heterogeneous phase, scales with the microstructural characteristic length ℓ. For systems with large L/ℓ ratios, region I should be considerably smaller than region III and therefore its presence may be insignificant in assessing initiation of crack growth. Under such small scale heterogeneity conditions, the mechanics of crack growth could be assessed based on the homogenized fields dominating the much larger region III. On the contrary, for layered systems wherein the L/ℓ ratio is relatively small, region III may not exist thus rendering the use of the homogenized orthotropic solutions inappropriate. For such systems, the near-tip asymptotics ought to be understood within the context of the lamination morphology and composite microstructure through more accurate and realistic studies.

In this work, a systematic finite element study is used to assess the effects of the heterogeneous layered microstructure on the near-tip asymptotics. The next section describes the finite element model that is used to study the effects of dual length ratio L/ℓ, constituent properties and volume fraction of fiber reinforcements, on the transition from the behavior dominated by region I to that dominated by region III.

3. Near-tip finite element model

While a realistic plane model for a laminated composite consists of plane strain conditions, plane stress conditions are assumed in order to reduce the number of required material properties. It is expected that the plane stress results will provide significant information regarding the effects of heterogeneity on the near-tip stress fields in a laminated composite. Consider the near-tip plane stress region shown in Fig. 4. The physical dimensions of this zone are $2Rx2R$ such that $R \leqslant r_3$, where r_3 signifies the boundary of region III consistent with Fig. 3. In this model, the actual lamination microstructure is retained. As shown in Fig. 4, a regular array of homogeneous linear elastic isotropic fiber layers of equal width denoted by ℓ is embedded within an otherwise homogeneous linear elastic isotropic matrix material. When accounting for fiber induced layer orthotropies, this arrangement is meant to represent a typical [0/90] fiber reinforced laminate composite.

As indicated above, the region under consideration includes the physical crack tip which for the sake of simplicity is taken to be within the matrix phase at the midpoint between two fiber layers. The crack surfaces are assumed to be traction free. Mode I loading is considered, so that only the upper half of the near-tip region is descretized in the finite element studies. In doing so, consistent geometric and traction symmetry conditions are imposed ahead of the crack such that the displacement components in the y direction at every node on the symmetry plane are restrained to zero while maintaining zero nodal force resultants in the x direction at each of the above nodes. As shown schematically in Fig. 4, on the remaining boundary of this heterogeneous near-tip region, the asymptotic mode I displacements corresponding to the homogeneous orthotropic solutions for the laminate composite are prescribed. These boundary displacements, driven by the applied $K_{\mathrm{I}}^{\mathrm{ortho}}$ have the following form

$$\begin{Bmatrix} u \\ v \end{Bmatrix} = K_{\mathrm{I}}^{\mathrm{ortho}} \sqrt{\frac{r}{2\pi}} \begin{Bmatrix} U(\theta, \mu_1, \mu_2) \\ V(\theta, \mu_1, \mu_2) \end{Bmatrix}, \tag{1}$$

where r and θ are the polar coordinates consistent with Fig. 2, u and v represent the displacement components in the x and y direction respectively, and U and V are the spatial eigenfunctions obtained by solving the near-tip mode I asymptotic problem for an orthotropic medium. The explicit forms for U and V are given in the Appendix.

It should be understood that this model does not incorporate finite geometry characteristics. In other words, R does not directly represent a macro-length, rather it provides an indirect measure of a macroscopic characteristic length as discussed later on in this section. As discussed earlier, this model's aim is to study the evolution of the stress fields within the singular domain in relation to the laminate heterogeneities. Thus, the only requirement on R is that stated earlier, i.e. $R \leq r_3$, where r_3 is shown on Fig. 3 and represents the outermost boundary of the singular orthotropic domain in the crack tip region. Consistent with this objective, the near-tip boundary value problem is defined as discussed above at fixed R values. For a given fiber volume fraction, various lamination morphologies corresponding to laminates with different L/ℓ ratios are modeled by changing the number of fiber layers placed over the fixed distance R. It is expected that this approach will capture the various near-tip asymptotics and the transitional characteristics from region I to region III through region II. This procedure establishes critical limits on the dual length ratio L/ℓ for which orthotropic volume average stresses and stress intensities can be used to represent with sufficient accuracy the near-tip stress fields in composite laminates. The relation between R and the macro length L is currently being investigated by the authors using finite geometries. It is expected however,

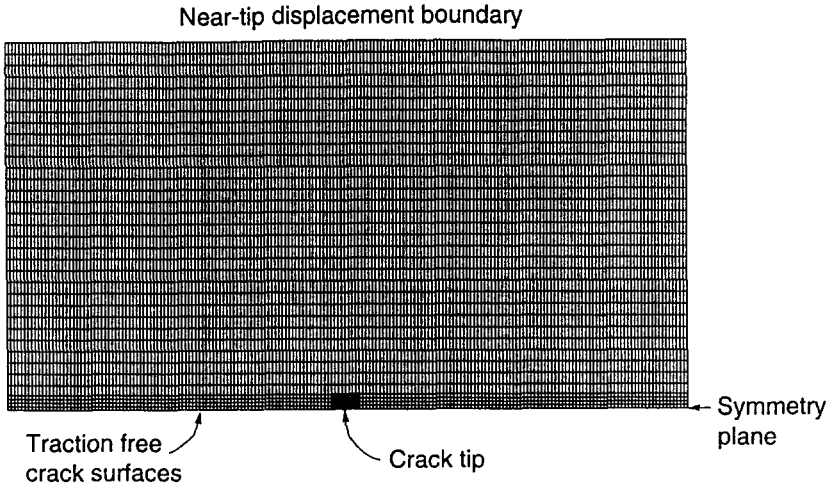

Fig. 5a. A typical finite element mesh used in solving the near-tip boundary value problem shown in Fig.4.

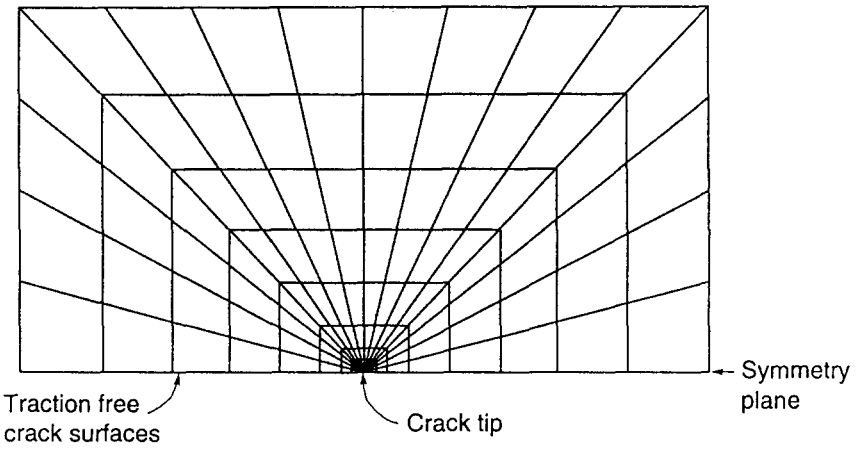

Fig. 5b. Detail of the focused near-tip finite element mesh.

that the macro length is of the order 10–20 R and it is sensitive to both the dual length ratio L/ℓ and the degree of material heterogeneity. This point will be discussed subsequently in the results and discussion sections.

The finite element mesh used in this study is shown in Fig. 5. The mesh is composed of eight-noded quadrilateral plane stress elements with four stations for the integration of the element stiffness. The meshes were developed in accordance with the layered morphology shown in Fig. 4, which was implemented by assigning the corresponding matrix or fiber material properties to the respective finite elements. In order to investigate the effects of the dual length ratio L/ℓ various meshes were constructed. In all cases, a focused mesh located entirely within the matrix phase, as shown in Fig. 5, was used in the vicinity of the crack tip. The crack tip was surrounded by a rosette of singular quarter-point elements. As explained in the Appendix, these elements were employed to capture the square root singularity in stresses, and to allow calculation of the J-integral in the near-tip region. The tip stress intensity

factor, $K_{\mathrm{I}}^{\mathrm{tip}}$ and the associated energy release rate $\mathcal{G}_{\mathrm{tip}}$ were independently calculated using the displacement correlation technique [23–25] and the J-integral [26].

The idea behind this simplified model is as follows. This model implicitly assumes that the $K_{\mathrm{I}}^{\mathrm{ortho}}$ region or annular region III exists around the crack tip. If L/ℓ is sufficiently large to warrant homogenization, then the volume averaged stresses calculated using the heterogeneous finite element model should be close to those predicted by the $K_{\mathrm{I}}^{\mathrm{ortho}}$ dominated singular solution. On the other hand, if L/ℓ is relatively small, which implies that the heterogeneous zone is composed of only few in number but rather large fibers, the $K_{\mathrm{I}}^{\mathrm{ortho}}$ dominated region will be engulfed by the transition region introduced by the heterogeneity, and the calculated displacements will not approach those predicted by (1). The results of the calculations are presented in the next section.

4. Results

Mesh sensitivity studies suggested that in order to capture the near-tip fields accurately, 128 elements were needed in the focused region. This was determined by comparing the J-integral calculated using the displacement correlation technique with the corresponding value calculated using Park's virtual crack extension method (see Appendix).

Numerical finite element calculations were performed for $E_f/E_m = 2, 10$ and $\nu_f = \nu_m = 0.3$, where the subscripts f and m denote properties for the fiber and matrix phases respectively. These are typical values for a ceramic matrix composite and a polymer or metal matrix composite respectively. Two fiber volume fractions have been considered: $v_f = 0.2$ and $v_f = 0.5$. For each of the above material combinations, the dual length ratio was varied from $R/\ell = 10$ to $R/\ell = 100$. The numerical results are presented in three different ways: actual stress σ_{yy} ahead of the crack as a function of distance from the crack tip, *unit cell* stress $\bar{\sigma}_{yy}$ ahead of the crack as a function of distance from the crack tip, and angular variation of actual stresses, i.e., σ_{xx}, σ_{yy}, σ_{xy} at two fixed radial distances from the crack tip within region I and III respectively.

4.1. Normal stress profiles ahead of the crack tip

Figures 6 and 7a through 7d show actual stress profiles for the stress component σ_{yy} ahead of the crack tip. As indicated on the figures, these results were obtained for a composite laminate with fiber volume fraction $v_f = 0.5$, modulus ratio $\frac{E_f}{E_m} = 10$ and dual length ratios $\frac{R}{\ell} = 10, 16.67, 25, 50$, and 100. The results were nondimensionalized and plotted using a *Log-Log* scale, so that the slope of the stress profile indicates the strength of the dominant singularity. The stresses shown in Fig. 6 represent actual stress measures numerically predicted at element integration stations close to the symmetry plane. This is clearly reflected through the discrete character of the reported results. For comparison purposes, the analytical homogeneous orthotropic predictions were also plotted as a solid line. As expected, the pointwise σ_{yy} stress component predicted via the method of finite elements is discontinuous at all fiber/matrix interfaces consistent with the modulus mismatch between the fiber and matrix phases. The elastic stresses within the softer matrix phase are consistently lower than the orthotropic predictions, whereas those within the fiber or stiffer phase are higher. It is observed that consistent stress patterns emerge. For all R/ℓ ratios, the overall stress pattern when viewed over the entire distance R in both the fiber and matrix phases seems to be $r^{-1/2}$ singular. This becomes apparent when connecting the mid-point stress predictions at

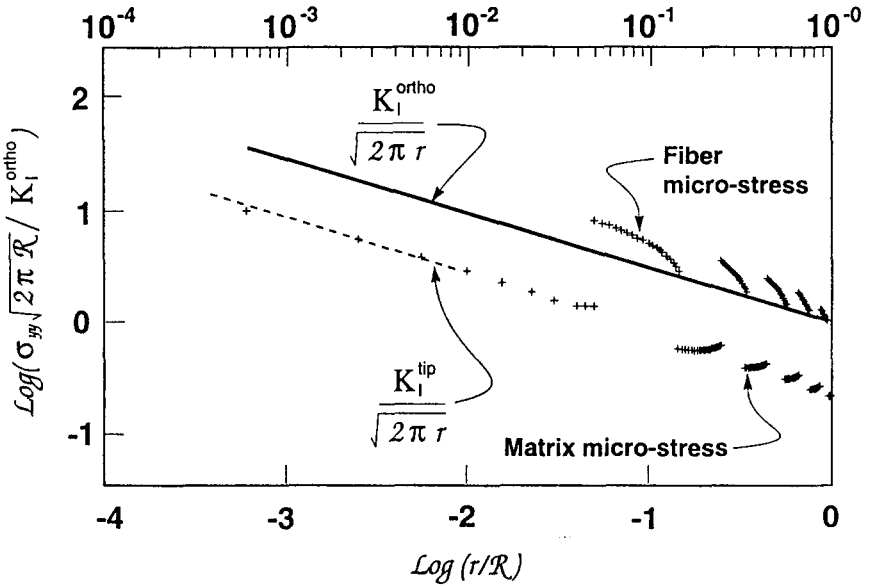

Fig. 6. Normal stress profile ahead of the crack tip predicted via the method of finite elements. These plane stress results were obtained for a system with dual length ratio $R/\ell = 10$, elastic moduli ratio $E_f/E_m = 10$ and fiber volume fraction $v_f = 0.5$.

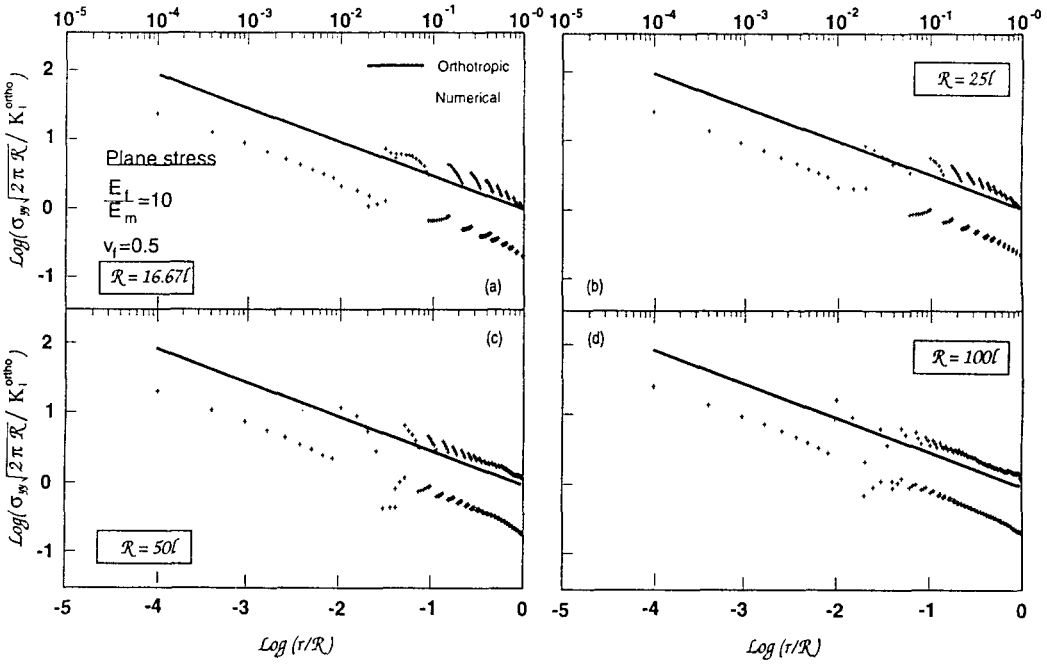

Fig. 7. Normal stress profiles ahead of the crack tip predicted via the method of finite elements. The solid lines represent the homogeneous orthotropic predictions whereas the symbols represent finite element results.

the fiber and matrix phases respectively, with a straight dash line as shown in Fig. 6. This line is parallel to the orthotropic solid line indicating similar overall singular character. Clearly, if such separable singular fields are found to dominate the stresses in the fiber and the matrix

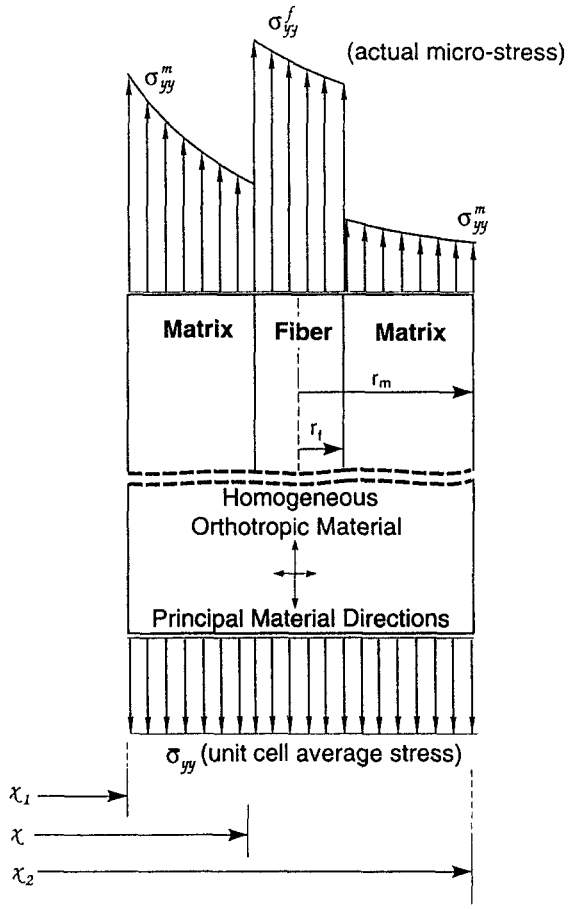

Fig. 8. A schematic representation of the unit cell average stresses obtained using the actual fiber and matrix micro-stresses averaged over the length of the unit cell, in accordance with (2).

phases respectively, distinct stress intensities such as $K_{\mathrm{I}}^{f}\big)_{y}$ and $K_{\mathrm{I}}^{m}\big)_{y}$ may be defined in order to account for the stress intensity difference dominating the σ_{yy} stresses in the fiber and matrix phases respectively. Such observations may provide useful insights in postulating and/or reconstructing analytically the near-tip stress fields for cracks embedded in composite laminates similar to that shown in Fig. 1.

Although the stresses reported in Figs. 6 and 7 represent actual micro-stresses developed in the fiber and matrix phases, an alternative stress measure, namely the volume average stress, is employed to compare the model's predictions with the near-tip homogeneous orthotropic asymptotic results, and to assess the effects of dual length ratio on the near-tip stress fields. A typical *unit cell* subjected to discontinuous stresses consistent with Figs. 6 and 7 is shown in Fig. 8. For planar problems, the volume average stress or *unit cell* stress, i.e. $\overline{\sigma}_{yy}$ is defined with the aid of Fig. 8 as follows

$$\overline{\sigma}_{yy} = \frac{1}{x_2 - x_1} \int_{x_1}^{x_2} \sigma_{yy}(x)\,\mathrm{d}x, \tag{2}$$

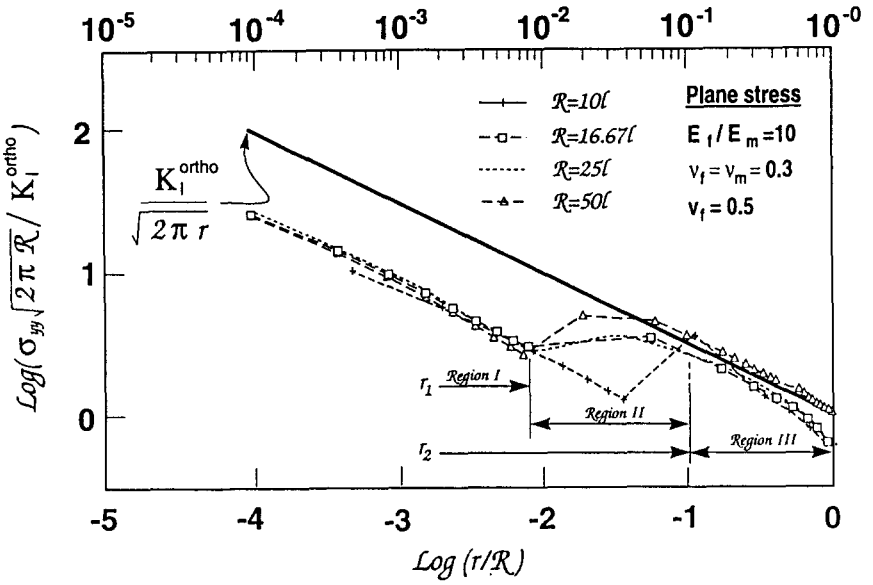

Fig. 9. Normal unit cell stress profiles ahead of the crack tip predicted via the method of finite elements. For all systems considered, the matrix stresses in region I surrounding the crack tip are $r^{-(1/2)}$ singular. Systems with $R/\ell < 25$ appear to deviate the most from the orthotropic results in region III.

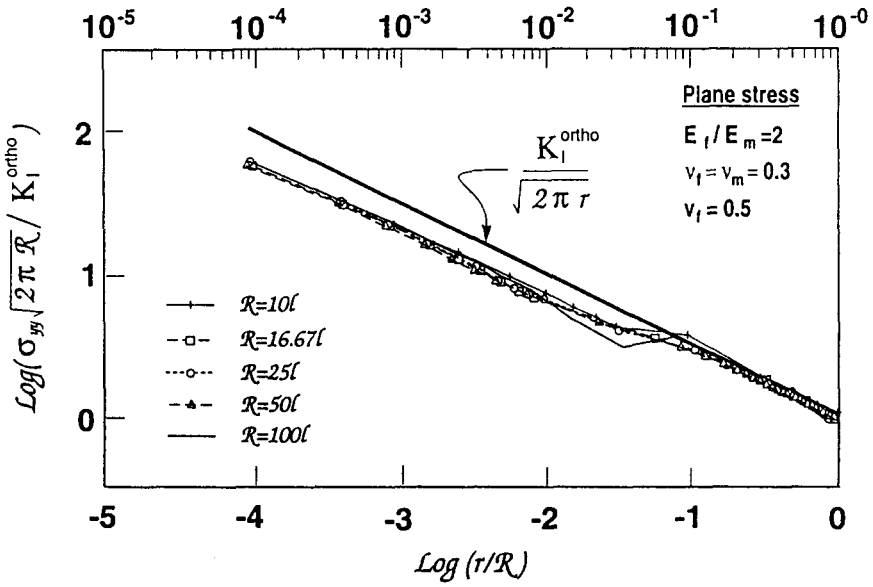

Fig. 10. Normal unit cell stress profile ahead of the crack tip predicted via the method of finite elements. A lower modulus mismatch results in smaller deviations from the orthotropic predictions in region III.

where $x_2 - x_1$ denotes the width of the unit cell over which $\overline{\sigma}_{yy}$ is applied, and $\sigma_{yy}(x)$ denotes the pointwise stress which varies with position x within the unit cell as shown schematically in Fig. 8. Figure 9 shows the *unit cell* predictions obtained using the same results that were presented in Figs. 6 and 7 above.

It is observed that, the matrix stresses in the near-tip region within region I (see Fig. 3), are $r^{-1/2}$ singular consistent with the singular fields around cracks embedded in homogeneous

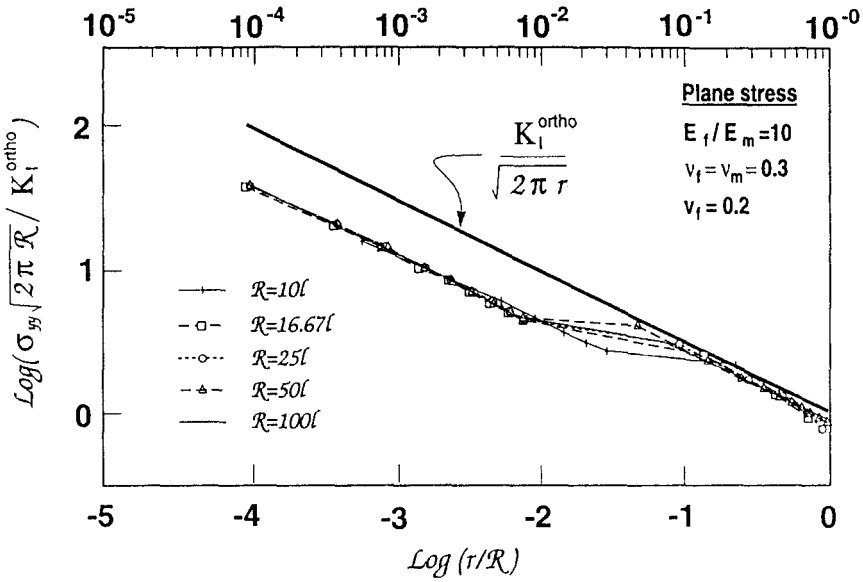

Fig. 11. Normal unit cell stress profiles ahead of the crack tip predicted via the method of finite elements. When compared to the results reported in Fig. 9, these results in region III are in closer agreement with the homogeneous orthotropic predictions. This apparently is due to the lower volume fraction of heterogeneities used.

systems. Outside region I, the above stress fields exhibit a transition region consistent with region II discussed earlier in this work. The extent of the transitional stress profile appears to depend on composite microstructural aspects such as fiber volume fraction, fiber/matrix elastic mismatch and the composite dual length ratio $\frac{R}{\ell}$ as depicted through Fig. 9 and Figs. 10–12. The effects of $\frac{R}{\ell}$ become more apparent when taking into consideration that the unit cell stress profiles reported in Figs. 9-12 are plotted using a *Log-Log* scale. For example, the unit cell stresses in systems with relatively large $\frac{R}{\ell}$ ratios, i.e. $\frac{R}{\ell} = 50$ consistently appear to converge to the orthotropic asymptotic results reported using the heavy line. On the contrary, and as shown in Fig. 9, an appreciable discrepancy appears to exist between the orthotropic asymptotic results and the unit cell stresses corresponding to laminates with $\frac{R}{\ell}$ smaller than 25. This effect is especially pronounced for the $\frac{R}{\ell} = 10$ system. Similar but not as pronounced trends are exhibited by the other composite laminates considered in this study and reported in Figs. 10–12. As expected, the effects discussed above diminish with decreasing material mismatch and fiber volume fraction. Thus, in systems elastically similar to those considered in this study and with $\frac{R}{\ell} > 25$, one may conclude that a well defined region III exists wherein the finite element stress predictions exhibit the expected $r^{-1/2}$ with the $K_{\mathrm{I}}^{\mathrm{ortho}}$ being the characterizing parameter.

In order to explore further the structure of the near tip fields, the angular variations of stress components σ_{yy}, σ_{xx} and τ_{xy} are presented in Figs. 13–20. The results were obtained at radial distances very close to the crack tip within region I as well as far away from the crack tip but still in the singular domain within region III. The results corresponding to region I are presented next.

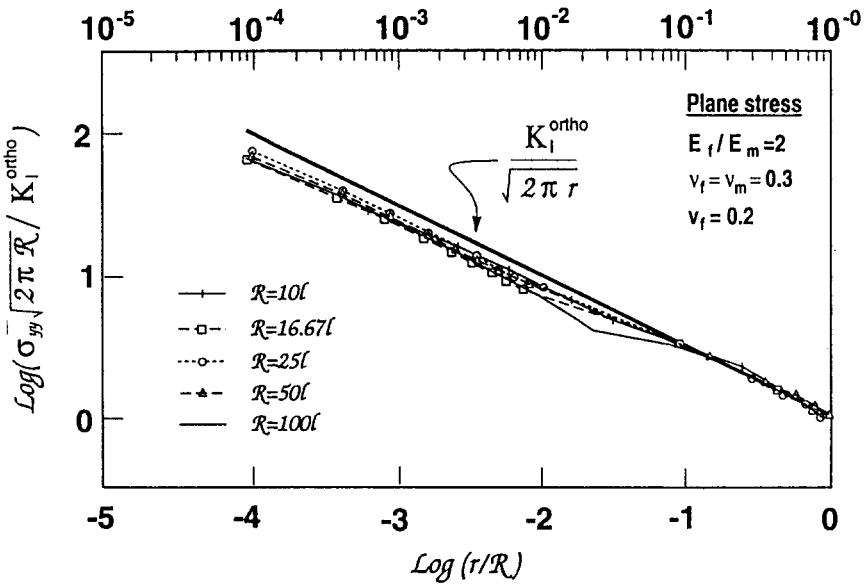

Fig. 12. Normal unit cell stress profiles ahead of the crack tip predicted via the method of finite elements. The influence of the heterogeneities on the near tip stress field becomes less significant with decreasing fiber/matrix modulus ratio and fiber volume fraction.

4.2. Angular variation of stress fields in region I

The angular variations of σ_{yy}, σ_{xx} and τ_{xy} are presented in Figs. 13–16. As indicated in Fig. 13, these results were obtained at a radial distance from the crack tip equal to $r = 0.009R$ within region I. The results reported in Figs. 13 and 14 correspond to composite systems with fiber volume fraction $v_f = 0.2$ and fiber/matrix modulus ratio $E_f/E_m = 2$ and 10 respectively.

In addition, the left column results, i.e. Figs. 13a–13c and Figs. 14a–14c were obtained for composite laminates for which $\frac{R}{\ell} = 16$ whereas the results on the right hand-side column, i.e., Figs. 13d–13f and 14d–14f are for laminates for which $\frac{R}{\ell} = 50$. Since for both Figs. 13 and 14, the fiber volume fraction is the same, i.e. $v_f = 0.2$, the left column results in both of the above figures correspond to laminates containing fewer in number but relatively thicker heterogeneous fibers when compared to those laminates corresponding to the right hand-side column results. Results, similar to those reported in Figs. 13 and 14, which were obtained for $v_f = 0.5$ are reported in Figs. 15 and 16.

In each of the above figures, and for comparison purposes, the orthotropic and homogeneous isotropic stress predictions are plotted together with the numerical finite element results obtained with the aid of the current model. In addition, all graphs include the isotropic near-tip solutions scaled with a local stress intensity factor K_I^{tip}. This K_I^{tip} was calculated to match the σ_{yy} numerical results at $\theta = 0$ within region I consistent with Fig. 6. The resulting ratio of the applied K_I^{ortho}/K_I^{tip} is reported in the corresponding figures for each system considered. All stress components were normalized using the characteristic stress $\hat{\sigma}_c = K_I^{ortho}/\sqrt{\frac{2\pi R}{1000}}$. As expected, the numerical results predicted in the matrix region surrounding the crack tip for all four systems considered, were found to be in excellent agreement for all values of θ, with those predicted for isotropic systems subjected to an effective mode I stress intensity factor equal to K_I^{tip} calculated as discussed above. It should be noted however, that these

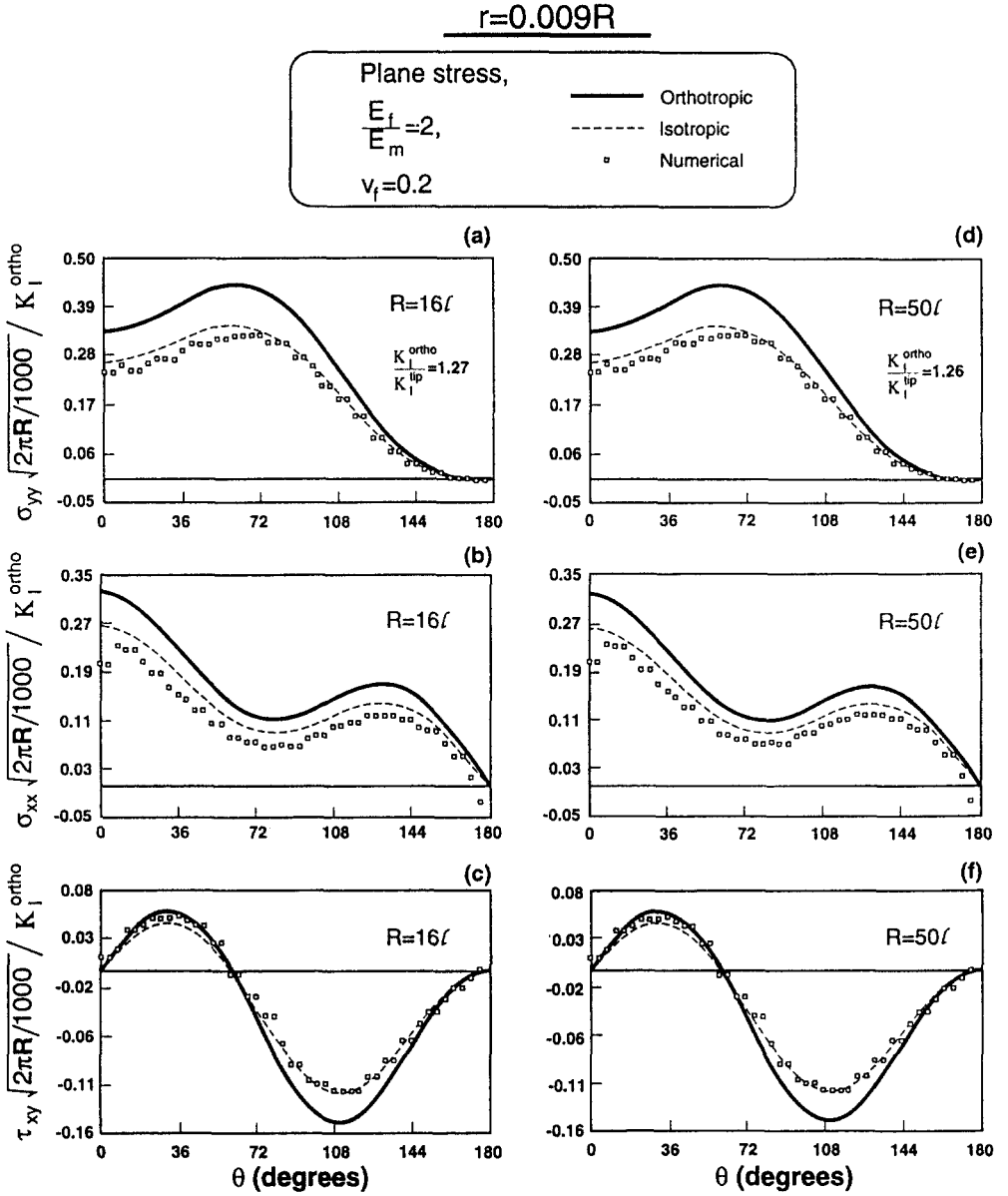

Fig. 13. Angular stress profiles in the matrix region I at radial distance $r = 0.009R$ from the crack tip. The isotropic stresses correspond to a mode I stress intensity factor which gives rise to normal matrix stresses ahead of the crack tip in region I consistent with those reported in Fig. 12.

fields also depend on the location of the crack tip relative to its first neighboring fiber inhomogeneity.

4.3. Angular variation of stress fields in region III

The angular stress profiles for σ_{yy}, σ_{xx} and τ_{xy} obtained at a distance $r = 0.8R$ from the crack within region III are presented in Figs. 17–20. These results are reported in a similar way as those presented for region I which were discussed above in conjunction with Figs. 13–

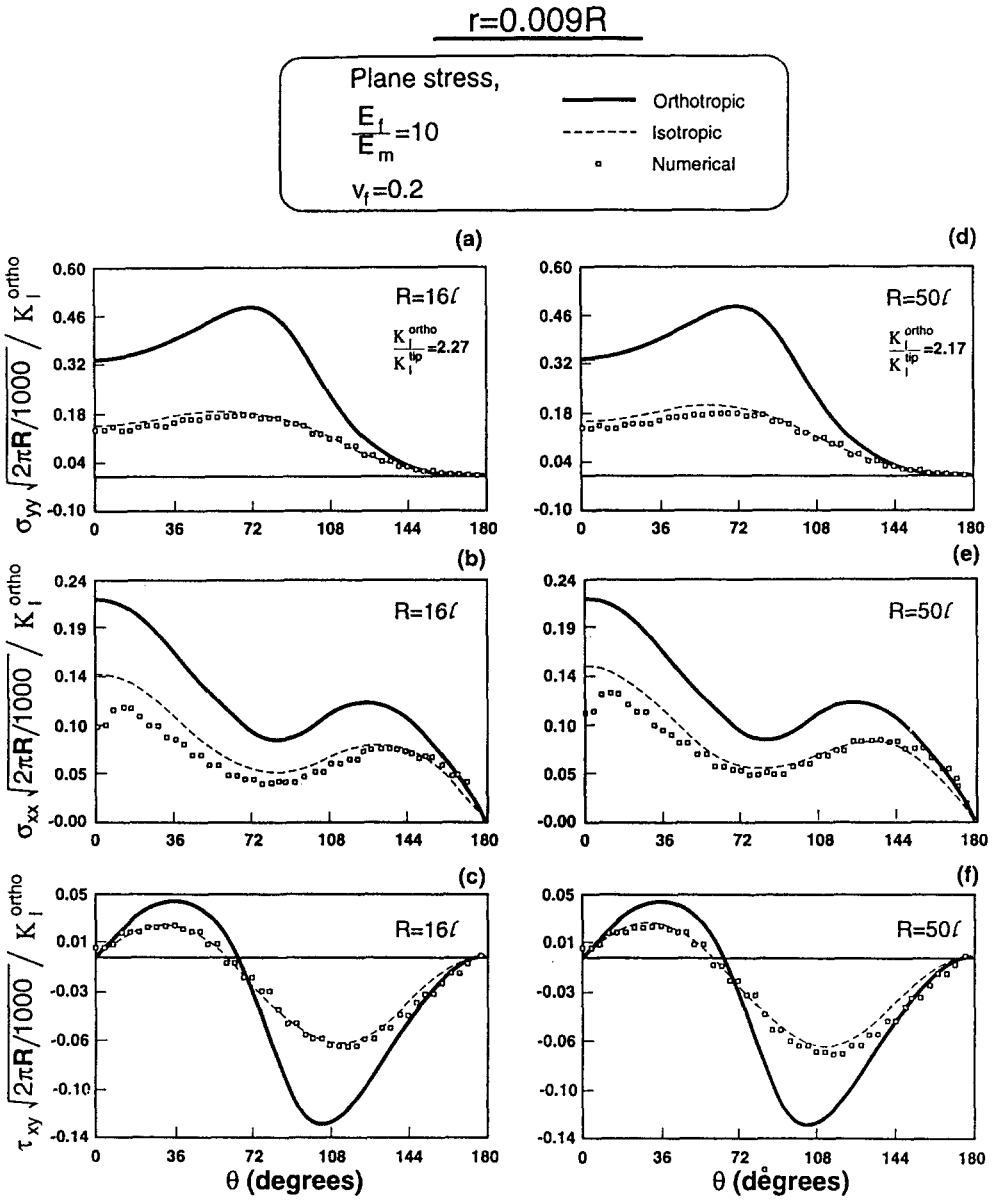

Fig. 14. Angular stress profiles in the matrix region I at radial $r = 0.009R$ from the crack tip. The isotropic stresses correspond to a mode I stress intensity factor which gives rise to normal matrix stresses ahead of the crack tip in region I consistent with those reported in Fig. 11.

16. Thus, the results reported in Figs. 17 and 18 were obtained for laminates for which $v_f = 0.2$ and $\frac{E_f}{E_m} = 2$ and 10 respectively, whereas Figs. 19 and 20 were obtained for laminates with $v_f = 0.5$ and $\frac{E_f}{E_m} = 2$ and 10 respectively. As before, in the above figures, the left column results were obtained using $\frac{R}{\ell} = 16$ while the right column results are for laminates wherein $\frac{R}{\ell} = 50$. Unlike the results reported for region I, these results do not compare to the homogeneous isotropic predictions which were not included in Figs. 17–20.

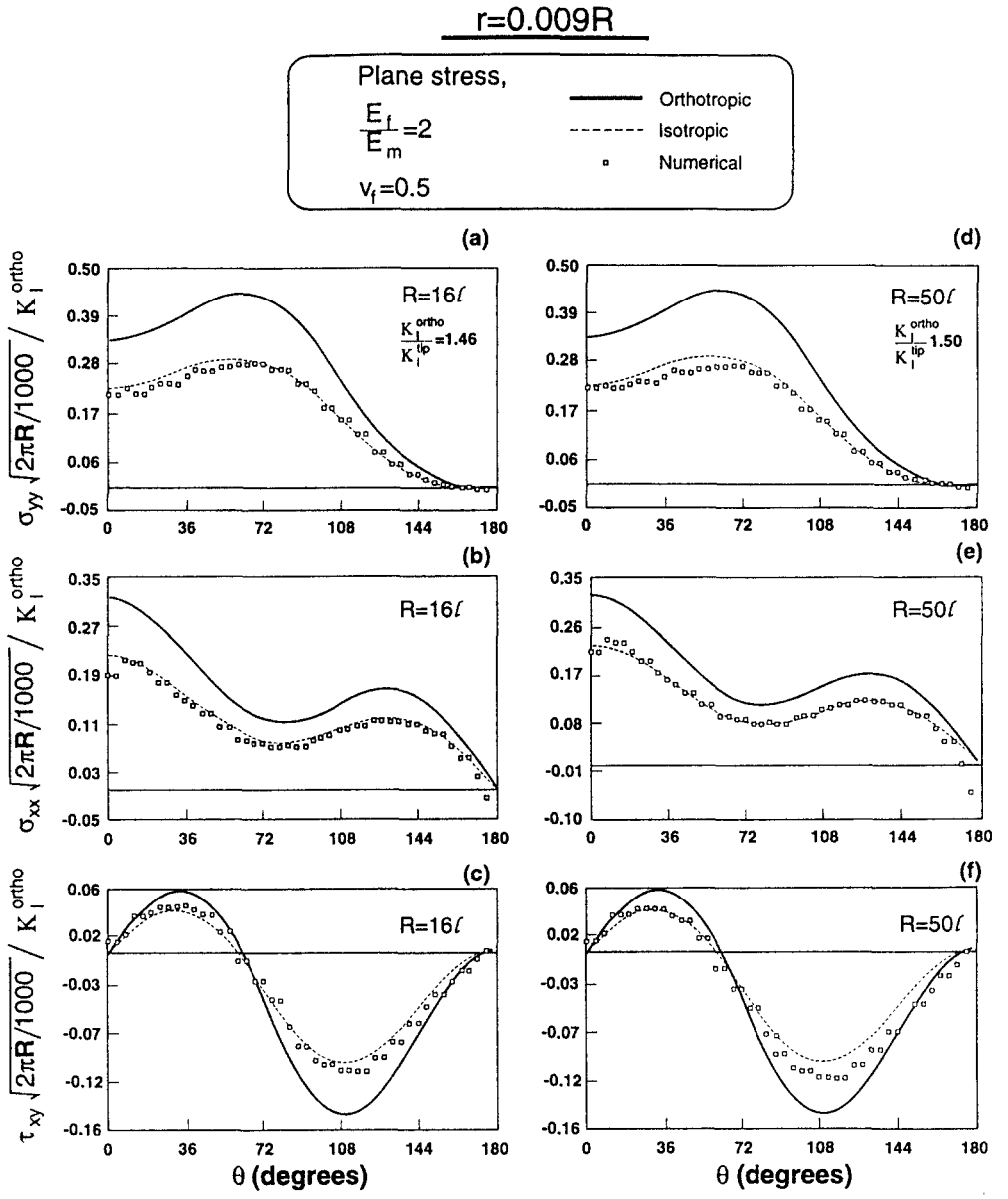

Fig. 15. Angular stress profiles in the matrix region I at radial distance $r = 0.009R$ from the crack tip. The isotropic stresses correspond to a mode I stress intensity factor which gives rise to normal matrix stresses ahead of the crack tip in region I consistent with those reported in Fig. 10.

In the latter figures, comparison is made between the finite element micro-stress results and the homogeneous orthotropic predictions.

As expected, for all four laminates considered, admissible stress discontinuities for the σ_{yy} stress component are predicted at every fiber/matrix interface due to the fiber/matrix elastic mismatch. Consistently, the fiber stresses were found to be higher than the orthotropic predictions whereas the stresses in the softer matrix material were found to be lower. These trends for σ_{yy} are shown as the top row of Figs. 17–20. Again, as expected, the stress jumps are greater for laminates with stronger fiber/matrix elastic mismatch.

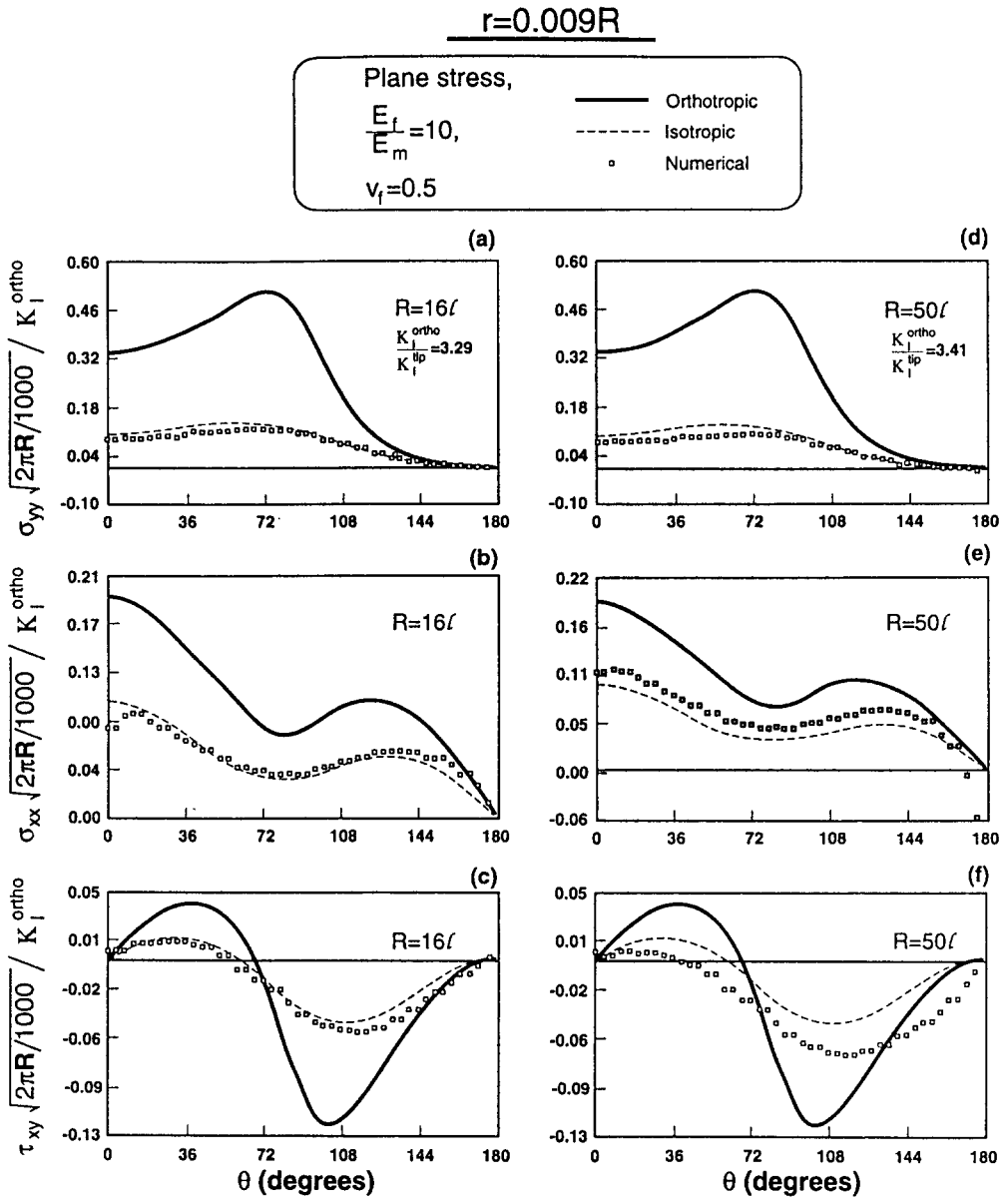

Fig. 16. Angular stress profiles in the matrix region I at radial distance $r = 0.009R$ from the crack tip. The isotropic stresses correspond to mode I stress intensity factor which gives rise to normal matrix stresses ahead of the crack tip in region I consistent with those reported in Figs. 6,7 and 9.

The angular profiles for the σ_{xx} and τ_{xy} stress components are reported as the second and third row in Figs. 17–20. Unlike σ_{yy}, these stresses are continuous with θ. It is of interest to notice that for systems with relatively weak elastic mismatch, i.e., $\frac{E_m}{E_f} = 2$, the finite element results were found to follow the orthotropic predictions very closely regardless of the dual length ratio $\frac{R}{\ell}$.

For systems with a stronger elastic mismatch, i.e., $\frac{E_m}{E_f} = 10$, the finite element results appear to deviate considerably from the orthotropic predictions. More specifically, consistently

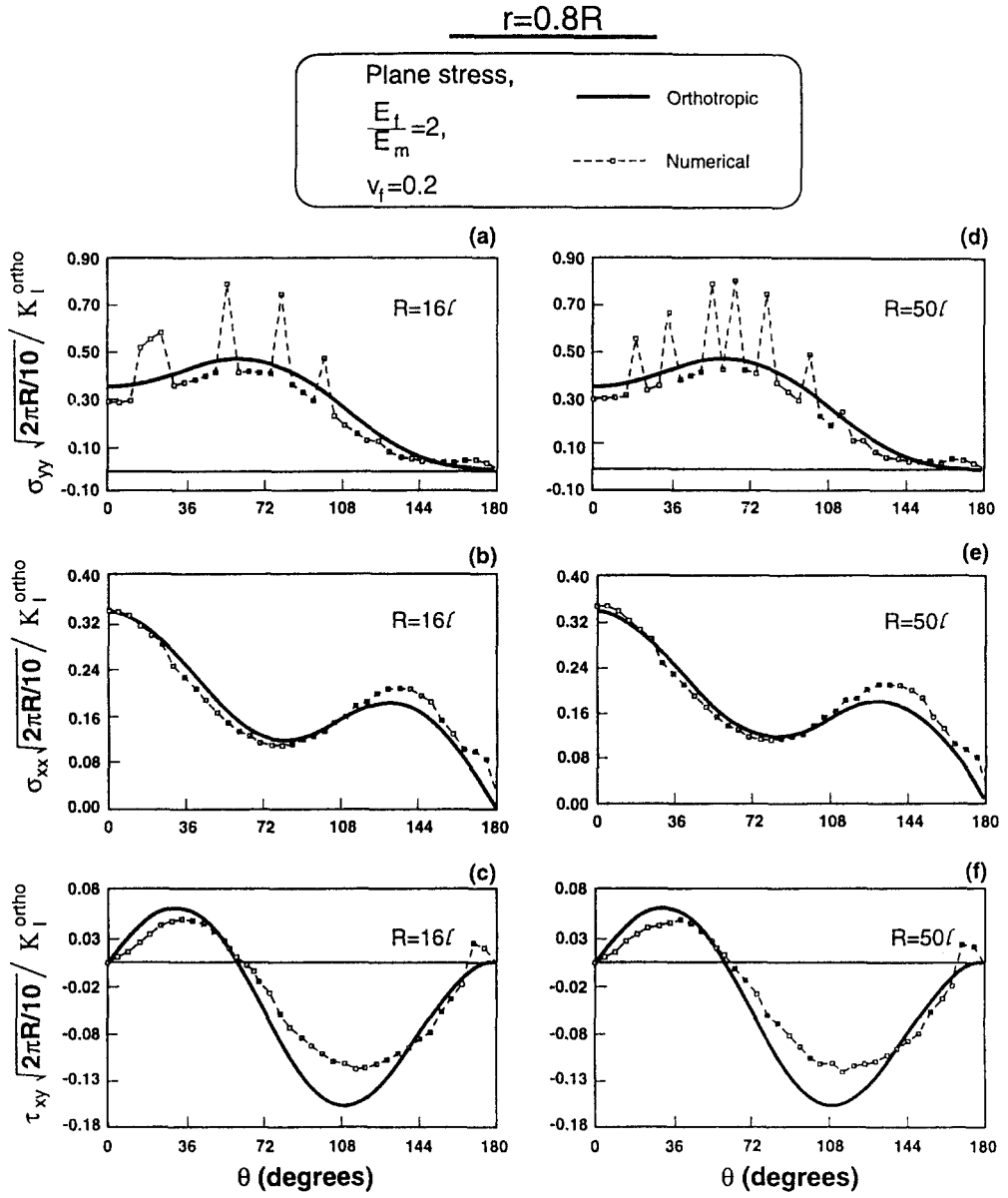

Fig. 17. Angular stress profiles in the matrix region III at radial distance $r = 0.8R$ from the crack tip.

lower values are predicted for the σ_{xx} stress component for almost the entire θ range while the overall stress profile appears to be similar to that obtained for orthotropic systems. Like σ_{xx}, the shear stress τ_{xy}, also appears to be lower in magnitude when compared to the orthotropic predictions. Its overall profile, however, appears to be similar to that obtained for homogeneous orthotropic systems. These results suggest that the extent of region III in composite laminates depends strongly on both the elastic mismatch as well as on the dual length ratio $\frac{R}{\ell}$.

In making the above comparisons, it should be noted that the numerical results reported in Figs. 17–20 represent pointwise microstresses. It is with this in mind that the apparent discrepancies of the finite element predictions from the homogeneous orthotropic results

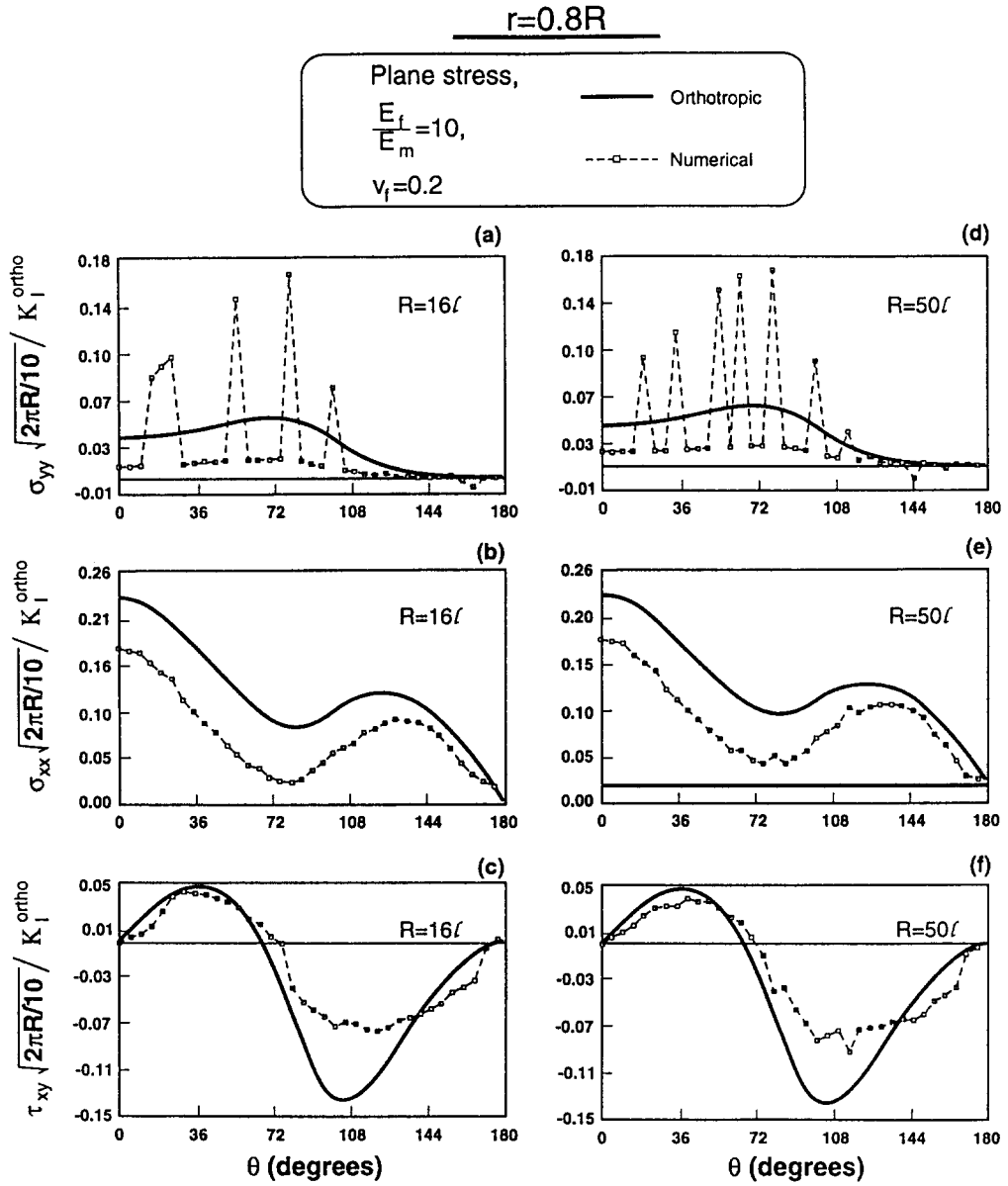

Fig. 18. Angular stress profiles in the matrix region III at radial distance $r = 0.8R$ from the crack tip.

ought to be understood. While this paper was in press, angular unit cell calculations were performed [27]. The results, which are not presented here, show trends similar to those observed in Figs. 9–12.

5. Discussion

This paper has shown, numerically, that the heterogeneity of size ℓ associated with a laminated structure containing a crack perpendicular to the reinforcement gives rise to asymptotics analogous to those in homogeneous materials undergoing nonlinear deformations. Calculations were performed by assuming that at a distance R from the crack tip, the volume average

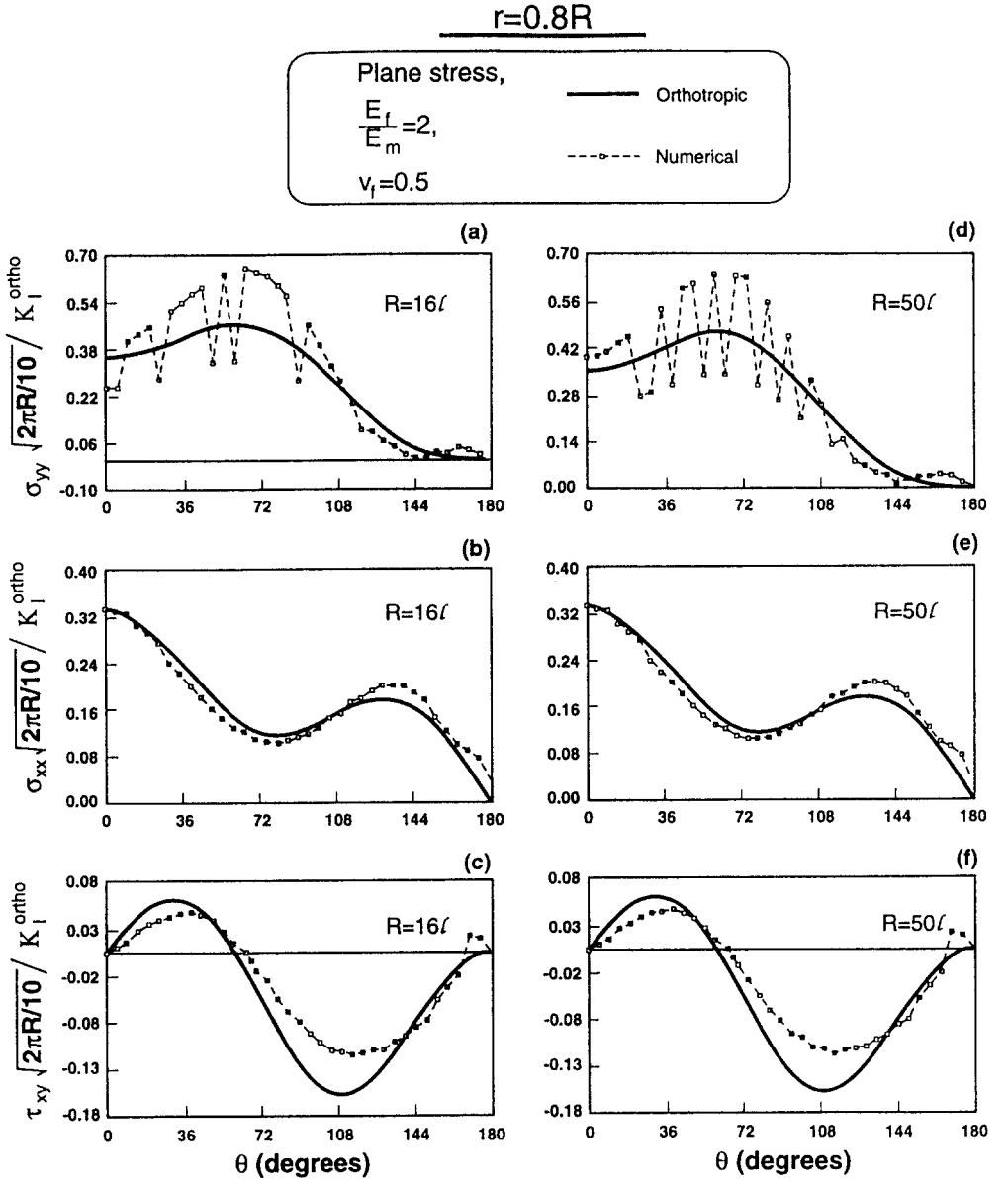

Fig. 19. Angular stress profiles in the matrix region III at radial distance $r = 0.8R$ from the crack tip.

stresses are dominated by the asymptotic solution for a cracked homogeneous orthotropic medium. The displacements corresponding to the homogenized problem were prescribed on the boundary of a finite element model which explicitly models the heterogeneous microstructure. The stress fields in composites with $R/\ell > 25$, i.e., laminates wherein the layer thickness is much smaller than the radius of the singular domain, were found to exhibit three distinct regions. Region I, which surrounds the crack tip, is dominated by a local stress intensity factor. For the systems considered, the stress fields within region I were found to be consistent with the homogeneous isotropic singular near tip fields. Outside region I the stress profiles revealed admissible discontinuities induced by the fiber/matrix elastic mismatch. However,

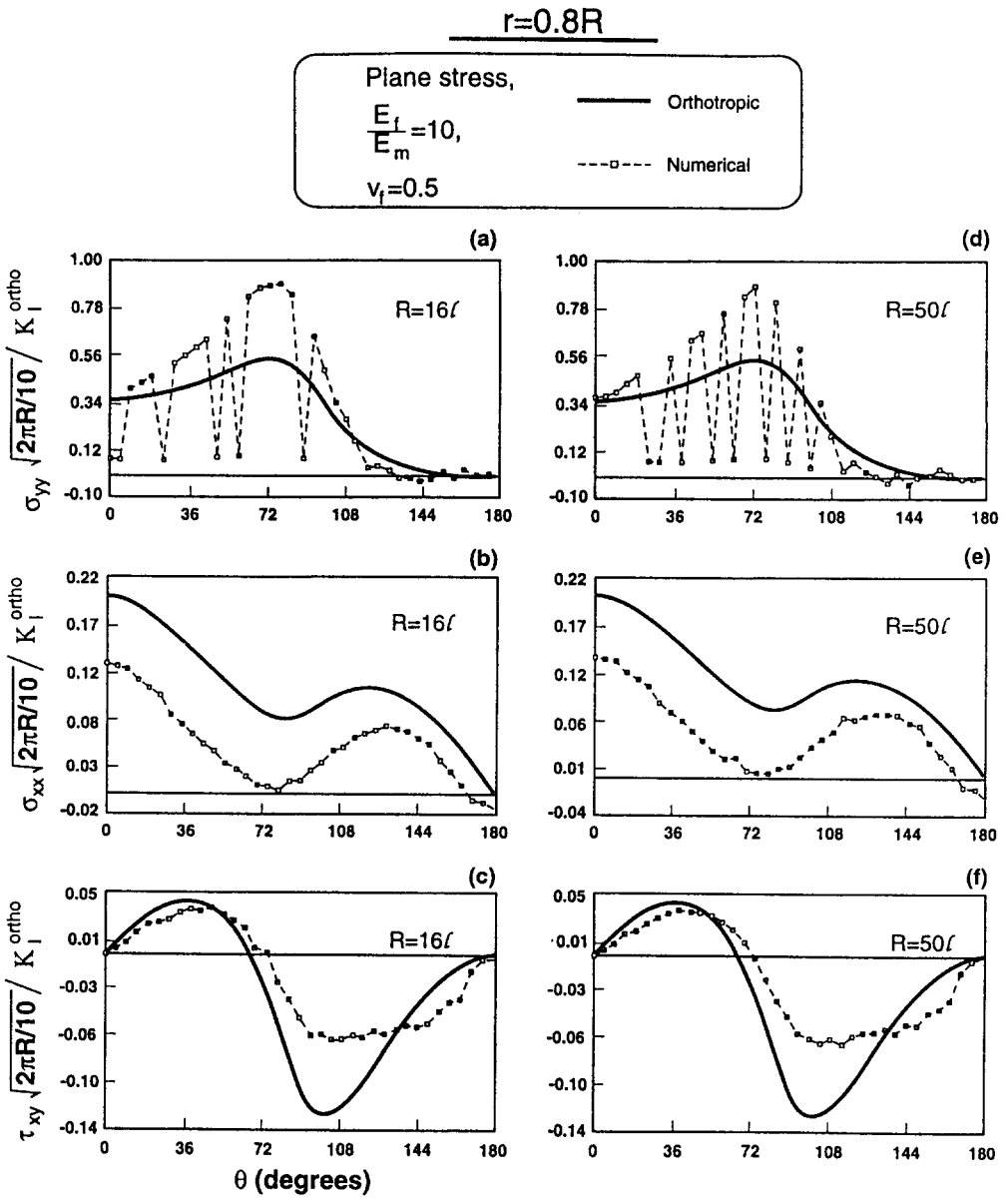

Fig. 20. Angular stress profiles in the matrix region III at radial distance $R = 0.8R$ from the crack tip.

the volume average stresses exhibited a continuous transition from region I through a transition region II, which appears to be limited to between one and three fibers ahead of the crack tip. The singularity of the associated transition stress fields appears to diminish with elastic mismatch, fiber volume fraction, and dual length ratio. In fact, nonsingular transition stress fields were obtained for certain laminate systems. Region II is in turn engulfed by region III, wherein the stress fields consistently were found to approach those predicted by the asymptotic solution for homogeneous orthotropic materials. Region III was found to dominate large portions of the near-tip singular domain extending over a large number of fibers/layers.

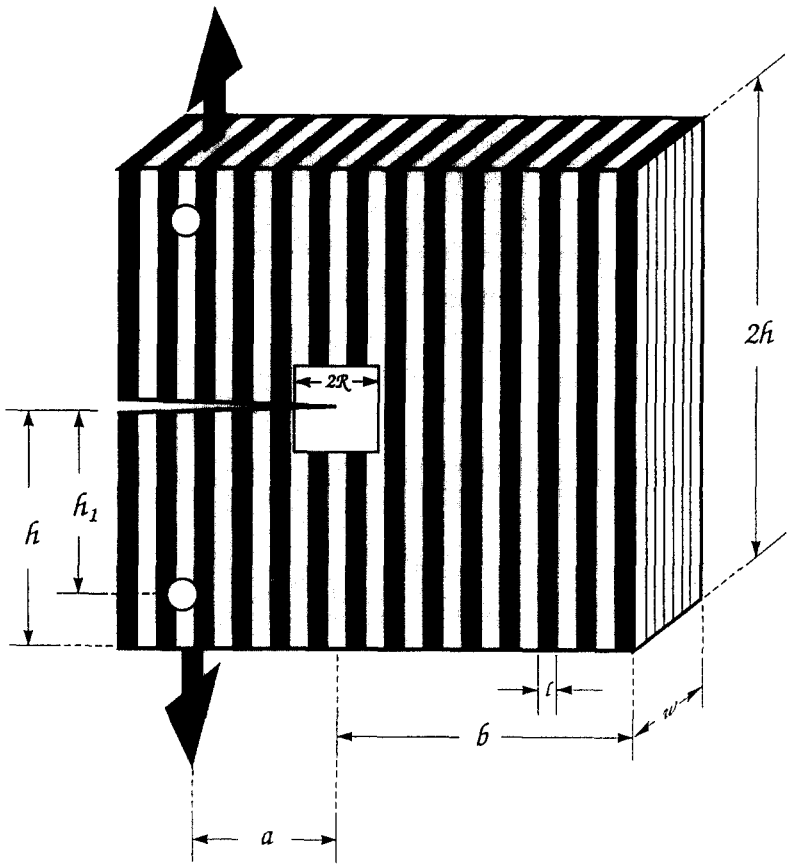

Fig. 21. A compact tension laminated beam proposed for the finite geometry dual- length ratio studies. The near-tip fields in the $2R \times 2R$ domain shown, will be monitored systematically consistent with the present study. Morphologies such as those shown in Fig. 22 could be included in the proposed studies.

Systems with $R/\ell < 25$, on the other hand, were found to exhibit well pronounced transition regions with little or no orthotropic regimes. For such systems the orthotropic stress intensity factor becomes meaningless. These results provide strong evidence that the relative size of the microstructure as well as its morphology and degree of material mismatch, may govern in a critical manner the evolution of the elastic stress and deformation fields in the near-tip domain. These, in turn, will strongly influence the development of whatever process zone results in the material system in the near tip domain.

The numerical model developed in this paper represents the first step in the development of numerical codes for simulating crack propagation in laminated composites, using a substructure approach. As such, this study has enhanced our understanding regarding the structure of the elastic near-tip fields and their complex relationship to the composite microstructure which is clearly needed in order to assess both qualitatively and quantitatively fracture in composite laminate systems. In the current study however, several simplifying assumptions have been made which limit the scope of the results. For example, in modeling the laminate constituents, the fiber/matrix phases have been assumed to be linear elastic and isotropic thus neglecting potential nonlinearities and inherent ply orthotropic characteristics. Stress induced, nonlinear processes such as plasticity or microcracking for example, may severely perturb

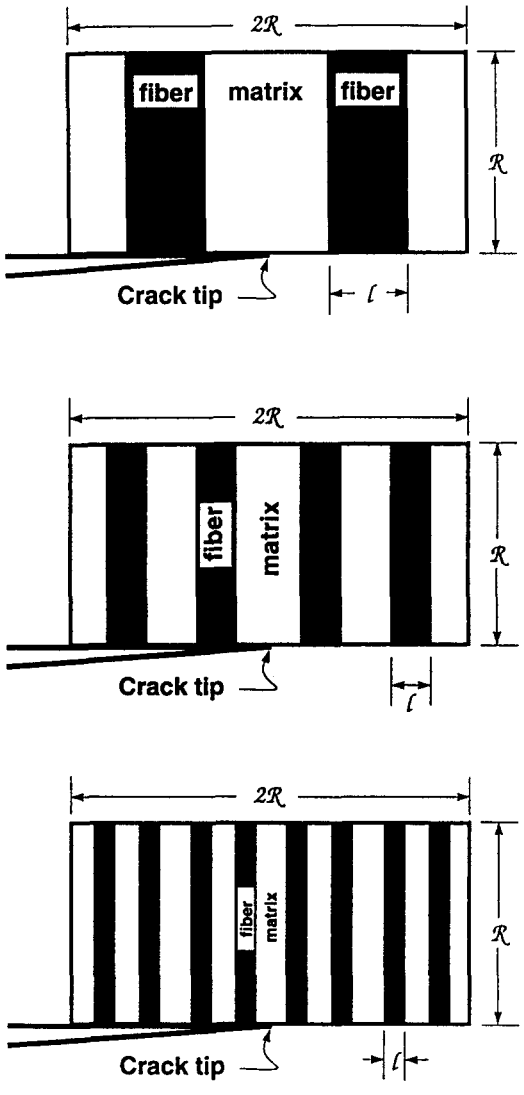

Fig. 22. Near-tip lamination morphologies at a fixed fiber volume fraction $v_f = 0.5$. (a) $R/\ell = 2$; (b) $R/\ell = 4$; (c) $R/\ell = 8$.

the elastic stress fields in the near tip region and may be critical in assessing crack growth behavior. In addition to the material modeling assumptions, and, in an effort to retain a degree of generality the study focused on the evolution of stress fields within the near-tip domain subjected to the asymptotic near-tip elastic displacements. As a result of this approach, the study has been limited to addressing finite geometry effects only indirectly through the size R of the singular domain which limits the ability of the current model to explore fully the dual length ratio effects on the evolution of the near-tip stress and deformation fields. Such an investigation, will require the use of a finite laminate geometry, say, the layered compact tension specimen shown in Fig. 21.

In such a study, wherein the number of layers and fiber volume fraction could vary from a very small to a very large number without any limitations, (see Fig. 22), the full dual-length scale effects could be captured by systematically monitoring the ensuing near-tip fields using methods similar to those used in this study.

In light of all of the above, the current study should be viewed as only the first step in an effort to enhance our understanding of fracture in composite laminates. As such, the methods, results and discussion reported in this study can be used to assist future complementary research in the field of fracture of laminated composite systems. This approach offers promise as a practical and relatively accurate method for analyzing and designing composite laminates.

6. Conclusions

The relationship between the laminate microstructure and the near-tip singular elastic stress fields has been studied numerically via the method of finite elements. A dual-length composite ratio has been introduced to account for the presence of two characteristic lengths, namely, the macrolength representing a macroscopic specimen dimension and the microlength representing a microstructural length. The stress fields and their respective region of dominance, were found to be sensitive to the elastic mismatch between the *fiber* and *matrix* phases, the volume fraction of fiber layers and the total number of layers placed in the singular domain.

This study suggests that homogenization procedures ought to be used with a great deal of caution, especially when dealing with heterogeneous laminates containing relatively low number of layers. The study provides evidence that, in the latter systems, the homogenized orthotropic singular stresses may not describe with sufficient accuracy the near tip stress fields which may require the use of finite geometry considerations.

Appendix

The following brief discussion presents some of the mechanics that is relevant to the work presented in the main body of the paper.

Constitutive relations of an orthotropic continuum

The inverse generalized Hooke's law for a linear elastic generally anisotropic material can be written using indicial notation as follows

$$\varepsilon_i = A_{ij}\sigma_j. \tag{A.1}$$

Matrix A_{ij} is a full six by six symmetric matrix containing the anisotropic compliance coefficients. For an orthotropic material oriented along its principal axis as shown in Fig. A1, uncoupling between tension and shear is obtained and the strain-stress relation become

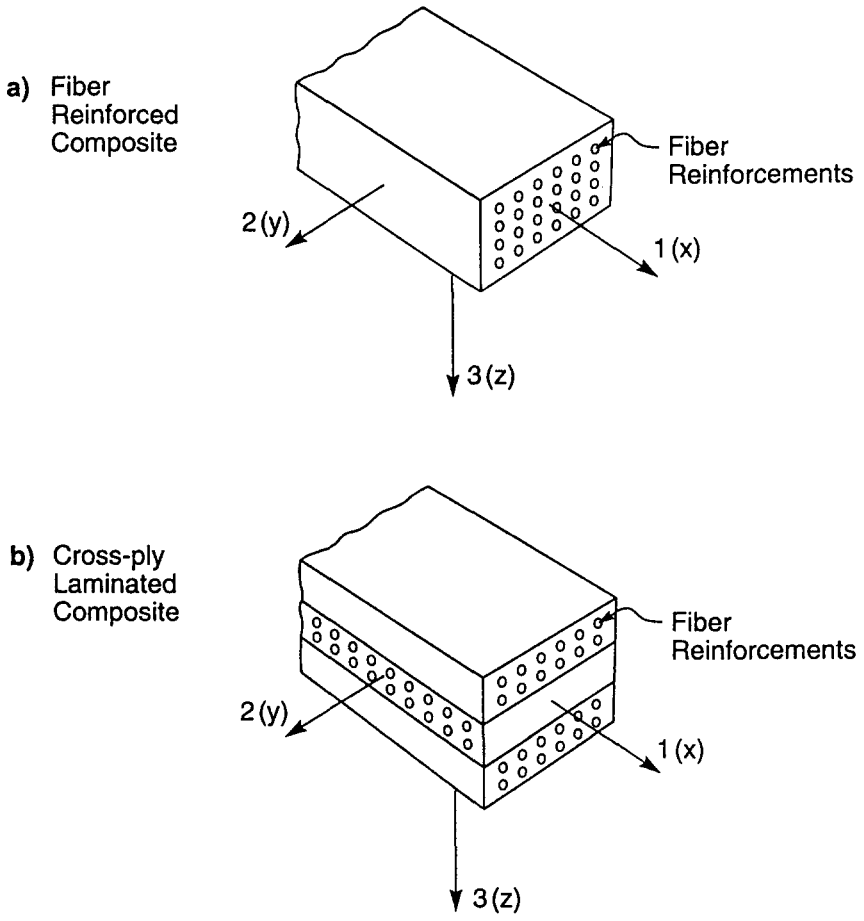

Fig. A1. Cross-sectional morphologies for (a) a fiber reinforced composite ply, and (b) a cross-ply composite laminae. The axis $1(x)$, $2(y)$ and $3(z)$ are used to denote the principal orthotropic material directions.

$$\begin{Bmatrix} \varepsilon_{xx} \\ \varepsilon_{yy} \\ \varepsilon_{zz} \\ \gamma_{yz} \\ \gamma_{zx} \\ \gamma_{xy} \end{Bmatrix} = \begin{bmatrix} \frac{1}{E_{11}} & \frac{-\nu_{12}}{E_{11}} & \frac{-\nu_{13}}{E_{11}} & 0 & 0 & 0 \\ \frac{-\nu_{21}}{E_{22}} & \frac{1}{E_{22}} & \frac{-\nu_{23}}{E_{22}} & 0 & 0 & 0 \\ \frac{-\nu_{31}}{E_{33}} & \frac{-\nu_{32}}{E_{33}} & \frac{1}{E_{33}} & 0 & 0 & 0 \\ 0 & 0 & 0 & \frac{1}{G_{23}} & 0 & 0 \\ 0 & 0 & 0 & 0 & \frac{1}{G_{31}} & 0 \\ 0 & 0 & 0 & 0 & 0 & \frac{1}{G_{12}} \end{bmatrix} \begin{Bmatrix} \sigma_{xx} \\ \sigma_{yy} \\ \sigma_{zz} \\ \sigma_{yz} \\ \sigma_{zx} \\ \sigma_{xy} \end{Bmatrix}. \tag{A.2}$$

In accordance with Fig. A1, E_{ii}, $i = 1,3$ are the elastic moduli in the principal $1,2,3$ directions, respectively, while G_{23}, G_{31}, and G_{12} are the shear moduli in the 2-3, 3-1 and 1-2 planes, respectively. The Poisson's ratios ν_{12}, ν_{13} and ν_{23} are defined such that $\nu_{ij} = -\varepsilon_{ii} / \varepsilon_{jj}$

due to an applied normal stress σ_{ii}. It follows from constitutive symmetry that $\nu_{ij} / E_{ii} = \nu_{ji} / E_{jj}$ for all permissible ij pairs.

For plane stress condition (A.2) reduces to

$$\begin{Bmatrix} \varepsilon_{xx} \\ \varepsilon_{yy} \\ \gamma_{xy} \end{Bmatrix} = \begin{bmatrix} \frac{1}{E_{11}} & \frac{-\nu_{12}}{E_{11}} & 0 \\ \frac{-\nu_{21}}{E_{22}} & \frac{1}{E_{22}} & 0 \\ 0 & 0 & \frac{1}{G_{12}} \end{bmatrix} \begin{Bmatrix} \sigma_{xx} \\ \sigma_{yy} \\ \sigma_{xy} \end{Bmatrix}. \tag{A.3}$$

The coefficients that appears in (A.3) are approximated in terms of the volume fraction of fibers v_f, the Young's moduli and Poisson ratios of the matrix and fiber (E_m, E_f, ν_m and ν_f) as follows

$$\begin{aligned} E_{11} &= v_f E_f + (1 - v_f) E_m, \\ E_{22} &= 1 / \left(v_f / E_f + (1 - v_f) / E_m\right), \\ \nu_{12} &= v_f \nu_f + (1 - v_f) \nu_m, \\ G_{12} &= 1 / \left(v_f / G_f + (1 - v_f) G_m\right). \end{aligned} \tag{A.4}$$

Crack tip fields in an orthotropic material

For the mode I loading considered in this paper, the stress field in the neighborhood of a crack tip in a linear elastic orthotropic material has the conventional square root singularity, which is characterized by the (orthotropic) stress intensity factor $K_{\mathrm{I}}^{\mathrm{ortho}}$. The stress and displacement components at a distance r from the crack tip are given by [28]

$$\begin{aligned} \sigma_{xx} &= \frac{K_{\mathrm{I}}^{\mathrm{ortho}}}{\sqrt{2\pi r}} \operatorname{Re}\left[\frac{\mu_1\mu_2}{\mu_1 - \mu_2}\left(\frac{\mu_2}{\sqrt{\cos\theta + \mu_2 \sin\theta}} - \frac{\mu_1}{\sqrt{\cos\theta + \mu_1 \sin\theta}}\right)\right], \\ \sigma_{yy} &= \frac{K_{\mathrm{I}}^{\mathrm{ortho}}}{\sqrt{2\pi r}} \operatorname{Re}\left[\frac{1}{\mu_1 - \mu_2}\left(\frac{\mu_1}{\sqrt{\cos\theta + \mu_2 \sin\theta}} - \frac{\mu_2}{\sqrt{\cos\theta + \mu_1 \sin\theta}}\right)\right], \\ \sigma_{xy} &= \frac{K_{\mathrm{I}}^{\mathrm{ortho}}}{\sqrt{2\pi r}} \operatorname{Re}\left[\frac{\mu_1\mu_2}{\mu_1 - \mu_2}\left(\frac{1}{\sqrt{\cos\theta + \mu_1 \sin\theta}} - \frac{1}{\sqrt{\cos\theta + \mu_2 \sin\theta}}\right)\right], \end{aligned} \tag{A.5}$$

$$u = K_{\mathrm{I}}^{\mathrm{ortho}} \sqrt{\frac{2r}{\pi}} \operatorname{Re}\left[\frac{1}{\mu_1 - \mu_2}\left[\mu_1 p_2 (\cos\theta + \mu_2 \sin\theta)^{\frac{1}{2}} - \mu_2 p_1 (\cos\theta + \mu_1 \sin\theta)^{\frac{1}{2}}\right]\right],$$

$$v = K_{\mathrm{I}}^{\mathrm{ortho}} \sqrt{\frac{2r}{\pi}} \operatorname{Re}\left[\frac{1}{\mu_1 - \mu_2}\left[\mu_1 q_2 (\cos\theta + \mu_2 \sin\theta)^{\frac{1}{2}} - \mu_2 q_1 (\cos\theta + \mu_1 \sin\theta)^{\frac{1}{2}}\right]\right],$$

where u and v represent the displacements in the x- and y-direction, respectively. In (A.5) $\mu_j = \alpha_j + i\beta_j$ ($j = 1, 2$) are the roots (with $\beta_j > 0$) of

$$A_{11}\mu^4 - 2A_{16}\mu^3 + (2A_{12} + A_{66})\mu^2 - 2A_{26}\mu + A_{22} = 0, \tag{A.6}$$

and

$$p_j = A_{11}\mu_j^2 + A_{12} - A_{16}\mu_j,$$
$$q_j = A_{12}\mu_j + A_{22}/\mu_j - A_{26}. \tag{A.7}$$

DISPLACEMENT CORRELATION TECHNIQUE

A square root singularity in strain can be introduced into a quadratic isoparametric element by the manipulation of the mid-side node positions. Barsoum [23] and Ingraffea and Manu [24] showed that by shifting the mid-side nodes to the quarter-point the displacement field along an edge of the element takes the form

$$u = A + B\sqrt{\frac{r}{l_e}} + C\frac{r}{l_e},$$
$$v = A^* + B^*\sqrt{\frac{r}{l_e}} + C^*\frac{r}{l_e}, \tag{A.8}$$

where A, B, C, A^*, B^* and C^* are functions of the nodal displacements, along the edge which corresponds to the crack surface, of the singular element of length l_e which emanates from the crack tip. These are presented in detail for the three dimensional case by Ingraffea and Manu [24].

By equating the square root terms in the asymptotic displacement equations in (A.5) with those given by (A.8), Saouma et al. [25] obtained the following stress intensity factor calibration equations

$$\begin{Bmatrix} K_{\mathrm{I}} \\ K_{\mathrm{II}} \end{Bmatrix} = \begin{bmatrix} f_{11}(\mu_1,\mu_2) & f_{12}(\mu_1,\mu_2) \\ f_{21}(\mu_1,\mu_2) & f_{22}(\mu_1,\mu_2) \end{bmatrix} \begin{Bmatrix} g_1(\mathrm{disp}_e) \\ g_2(\mathrm{disp}_e) \end{Bmatrix}, \tag{A.9}$$

where the functions f_{ij} and g_i $(i, j = 1, 2)$ represent, respectively, functions of relative anisotropy and nodal displacements. These can be recovered in [25].

ENERGY RELEASE RATE $\mathcal{G}$

For linear elastic fracture mechanics, the J-integral and the energy release rate $\mathcal{G}$ are synonymous. These are expressed in terms of the stress intensity factor by

$$J_{\mathrm{I}}^{\mathrm{tip}} = \mathcal{G}_{\mathrm{I}}^{\mathrm{tip}} = \frac{(K_{\mathrm{I}}^{\mathrm{tip}})^2}{E_{11}}. \tag{A.10}$$

This integral was calculated using the virtual crack extension technique option of ABAQUS as well as through the use of the calculated local stress intensity factor $K_{\mathrm{I}}^{\mathrm{tip}}$.

Acknowledgments

PGC was partially sponsored by the National Science Foundation through a Presidential Young Investigator award, grant No. CMS-9496209. Support was provided to R.B. and S.I. by NASA Lewis Research Center, grant No. NAG3-856.

References

1. J. Aveston, G.A. Cooper and A. Kelly, in *The Properties of Fiber Composites*, IPC Science and Technology Press, Guilford, England (1971) 15–26.

2. D.B. Marshall, B.N. Cox and A.G. Evans, *Acta Metallurgica* 33 (1985) 2013-2021.
3. B. Budiansky, J.W. Hutchinson and A.G. Evans, *Journal of Mechanics and Physics of Solids* 34, No. 2 (1986) 176–189.
4. D.B. Marshall and B.N. Cox, *Acta Metallurgica* 35 (1987) 2607–2619.
5. B.N. Cox and D.B. Marshall, *Acta Metallurgica* 39 (1991) 579–589.
6. H. Luo and R. Ballarini, *Journal of Mechanics and Physics of Solids* 42, No. 2 (1994) 141–157.
7. P.G. Charalambides and A.G. Evans, *Journal of American Ceramic Society* 72: 5 (1989) 746–753.
8. A.G. Evans, M.Y. He and J.W. Hutchinson, in The Processing and Mechanical Properties of High Temperature/High Performance Composites, Annual Report, Department of Materials, University of California, Santa Barbara, 1990.
9. O. Spaizero, P.G. Charalambides and A.G. Evans, *Journal of American Ceramic Society* 73: 7 (1990) 1936–1940.
10. P.G. Charalambides, *Journal of American Ceramic Society* 74: 12 (1991) 3066-3080.
11. P.G. Charalambides, Unpublished research.
12. J.R. Rice, in *Fracture, An Advanced Treatise*, H. Liebowitz (ed.), Academic Press (1968) 192–308.
13. G.R. Irwin, in *Encyclopedia of Physics*, Vol. 6, S. Flugge (ed.), Springer, Berlin (1958) 551–590.
14. A.G. Evans, A.H. Heuer and D.L. Porter, in *Fracture 1977, Vol. 1*, D.M.R. Taplin (ed.), Pergamon, Oxford (1977) 529.
15. M. Ruehle, N. Claussen and A.H. Heuer, *Journal of American Ceramic Society* 69: 3 (1986) 195-197.
16. J.J. Pepe, *Metals Engineering Quarterly* 16 (1976) 46.
17. R.M. McMeeking and N. Aravas, 'Models of Ductile Rupture', presented at the 10th National Congress of Applied Mechanics, Austin Texas, June 16–20, 1986.
18. A.S. Argon (ed.), *Topics in Fracture and Fatigue*, Springer-Verlag, New York (1992).
19. A.G. Evans, *Materials Science and Engineering* A105/106 (1988) 65–75.
20. A.G. Evans, *Ibid.* A107 (1989) 227–239.
21. J.R. Rice and G.F. Rosengren, *Journal of Mechanics and Physics of Solids* 16 (1968) 1–12.
22. J.W. Hutchinson, *Journal of Mechanics and Physics of Solids* 16 (1968) 13–31.
23. R.S. Barsoum, *International Journal of Numerical Methods in Engineering* 11 (1977) 85.
24. A.R. Ingraffea and C. Manu, *International Journal of Numerical Methods in Engineering* 15 (1980) 1427–1445.
25. V.E. Saouma and E.S. Sikiotis, *Engineering Fracture Mechanics* 25 (1986) 115–121.
26. D.M. Parks, *Computer Methods in Applied Mechanics and Engineering* 12 (1977) 353–364.
27. J. Mahendra and P.G. Charalambides, unpublished work (1995).
28. G.C. Sih, P.C. Paris and H. Irwin, *International Journal of Fracture Mechanics* 1 (1965) 189–203.